



**HAL**  
open science

# Climate Controls on the Interseasonal and Interannual Variability of the Surface Mass and Energy Balances of a Tropical Glacier (Zongo Glacier, Bolivia, 16°S): New Insights From the Multi-Year Application of a Distributed Energy Balance Model

P. Autin, Jean-Emmanuel Sicart, Antoine Rabatel, A. Soruco, R. Hock

## ► To cite this version:

P. Autin, Jean-Emmanuel Sicart, Antoine Rabatel, A. Soruco, R. Hock. Climate Controls on the Interseasonal and Interannual Variability of the Surface Mass and Energy Balances of a Tropical Glacier (Zongo Glacier, Bolivia, 16°S): New Insights From the Multi-Year Application of a Distributed Energy Balance Model. *Journal of Geophysical Research: Atmospheres*, 2022, 127 (7), 10.1029/2021JD035410 . hal-04381081

**HAL Id: hal-04381081**

**<https://hal.science/hal-04381081v1>**

Submitted on 8 Jan 2024

**HAL** is a multi-disciplinary open access archive for the deposit and dissemination of scientific research documents, whether they are published or not. The documents may come from teaching and research institutions in France or abroad, or from public or private research centers.

L'archive ouverte pluridisciplinaire **HAL**, est destinée au dépôt et à la diffusion de documents scientifiques de niveau recherche, publiés ou non, émanant des établissements d'enseignement et de recherche français ou étrangers, des laboratoires publics ou privés.



## RESEARCH ARTICLE

10.1029/2021JD035410

### Key Points:

- Seasons over Zongo Glacier can be identified using the distribution of the cloud radiative forcing
- October and November play a strong control on the interannual surface mass balance variability of Zongo Glacier
- Distribution of the precipitation events in time is key in controlling the melt rate

### Supporting Information:

Supporting Information may be found in the online version of this article.

### Correspondence to:

P. Autin,  
[philemon.autin@univ-grenoble-alpes.fr](mailto:philemon.autin@univ-grenoble-alpes.fr)

### Citation:

Autin, P., Sicart, J. E., Rabatel, A., Soruco, A., & Hock, R. (2022). Climate controls on the interseasonal and interannual variability of the surface mass and energy balances of a tropical glacier (Zongo Glacier, Bolivia, 16°S): New insights from the multi-year application of a distributed energy balance model. *Journal of Geophysical Research: Atmospheres*, 127, e2021JD035410. <https://doi.org/10.1029/2021JD035410>

Received 14 JUN 2021  
Accepted 22 MAR 2022



### Author Contributions:

**Conceptualization:** P. Autin, J. E. Sicart, A. Rabatel  
**Data curation:** A. Soruco  
**Methodology:** P. Autin, J. E. Sicart, A. Rabatel  
**Software:** R. Hock  
**Supervision:** J. E. Sicart, A. Rabatel, R. Hock  
**Validation:** P. Autin  
**Visualization:** P. Autin  
**Writing – original draft:** P. Autin  
**Writing – review & editing:** P. Autin, J. E. Sicart, A. Rabatel, R. Hock

© 2022. The Authors.

This is an open access article under the terms of the [Creative Commons Attribution License](https://creativecommons.org/licenses/by/4.0/), which permits use, distribution and reproduction in any medium, provided the original work is properly cited.

# Climate Controls on the Interseasonal and Interannual Variability of the Surface Mass and Energy Balances of a Tropical Glacier (Zongo Glacier, Bolivia, 16°S): New Insights From the Multi-Year Application of a Distributed Energy Balance Model

P. Autin<sup>1</sup> , J. E. Sicart<sup>1</sup>, A. Rabatel<sup>1</sup>, A. Soruco<sup>2</sup>, and R. Hock<sup>3,4</sup> 

<sup>1</sup>University Grenoble Alpes, CNRS, IRD, Grenoble-INP, Institut des Géosciences de l'Environnement (IGE, UMR 5001), Grenoble, France, <sup>2</sup>Facultad de Ciencias Geológicas, Universidad Mayor de San Andrés, La Paz, Bolivia, <sup>3</sup>Department of Geoscience, Oslo University, Oslo, Norway, <sup>4</sup>Geophysical Institute, University of Alaska, Fairbanks, AK, USA

**Abstract** The application of a distributed energy balance model over nine years at an hourly time step to a 20 × 20 m grid cell over Glacier Zongo (Bolivia, 16°S) enabled assessment of the climate factors that control the interseasonal and interannual variability of its surface mass balance. The model was validated by comparing the measured and simulated discharge at the outlet, albedo at the Automatic Weather Station, surface state and annual mass balance both glacier-wide and as a function of altitude. Analysis of the mean monthly energy fluxes highlighted the importance of the meteorological conditions over October and November on the variability of the annual surface mass balance. Two sensitivity analyses are presented, one of the distribution of precipitation over time which maintains a physical coherence between the different meteorological variables and one of the impact of prolonged periods of intense cloud radiative forcing on the surface mass balance. The distribution of precipitation events over time and their associated amounts are the main drivers of the interannual variability of the surface mass balance via an albedo feedback effect. Additionally, prolonged periods of negative cloud radiative forcing, specifically over the month of November, notably reduce the melt rate.

**Plain Language Summary** This study aimed at identifying the meteorological variables which control the seasonal and annual melt rates of a tropical glacier in Bolivia considering nine years of measurements at the hourly timescale. The analysis of the energy fluxes at the weather station has shown that the period between the austral winter and summer is the period during which most melt can be generated making it key in defining the annual melt rates. The analysis of the impact of measured meteorological variables on the melt rate has shown that it is the solar energy that controls most of it. The amount of solar energy available for melt is defined by the state of the glacier surface (snow, ice, debris) which controls the amount of reflected energy. In this context, the frequency of the snowfall events plays a key role in controlling the melt as frequent events imply a whiter glacier which is able to reflect most of the incoming solar energy. Similarly, because clouds can block large portions of solar energy, sustained cloud periods can play an important role in reducing the melt rate.

## 1. Introduction

In recent decades, both field observations and remote sensing have shown a trend of glacier retreat in tropical South America (e.g., Dussailant et al., 2019; Kaser, 1999; Masiokas et al., 2020; Rabatel et al., 2013; Seehaus et al., 2020; Soruco et al., 2009; Vincent et al., 2018), with specific mass losses over the last decades even larger than the global mean (e.g., Rabatel et al., 2013; Zemp et al., 2019). Previous studies have linked these mass changes to the high sensitivity of tropical glaciers to changes in moisture-related variables including precipitation, albedo, and cloudiness rather than directly to air temperature (e.g., Sicart et al., 2005). Bradley et al. (2009) found statistical correlations between mass changes and air temperature for the Quelccaya Ice Cap, however, these might result from the indirect effect of air temperature on the phase of precipitation (e.g., Gurgiser, Marzeion, Nicholson, Ortner, & Kaser, 2013). Hence, air temperature increase does not increase melt directly, but it may change the local hygric regime. In addition, most studies conducted to understand the complex climate-glacier

relationships in the tropics have been carried out with data acquired over a short period (Hurley et al., 2016; Litt et al., 2014; Maussion et al., 2015; Mölg et al., 2008, 2009; Prinz et al., 2016; Sicart et al., 2005; Wagon et al., 1999).

Glacier surface mass balance is controlled by the climate via energy and mass fluxes between the atmosphere and the glacier surface (e.g., Cuffey & Paterson, 2010). These fluxes are modulated by conditions specific to tropical glaciers, including small seasonal air temperature variations, marked cloud and precipitation seasonality, very high elevations, and pronounced sublimation (e.g., Nicholson et al., 2013; Prinz et al., 2016; Sicart et al., 2011). Understanding the relationship between mass and energy balances and identifying the key meteorological variables that control the glacier surface mass balance is crucial to better estimate past and future changes of these glaciers and their consequences, for example, on water availability for human consumption, irrigation, or hydroelectricity production (e.g., Soruco et al., 2015).

Several studies put forward different atmospheric/meteorological factors as being responsible for the interannual variability of the surface mass balance of tropical glaciers in the Andes (e.g., Abermann et al., 2014; Gurgiser, Marzeion, et al., 2013; Gurgiser, Mölg, Nicholson, & Kaser, 2013; Hastenrath, 1997; Maussion et al., 2015; Vuille et al., 2008). Some highlighted the importance of the onset of the wet season (Francou et al., 1995; Sicart et al., 2011). However, Ramallo (2013) found poor correlations between the surface mass balance and the onset or end of the wet season primarily due to the difficulty in precisely identifying the latter which generally starts between mid-November and January in the eastern Andes of Bolivia. Other studies (e.g., Francou et al., 2004; Rabatel et al., 2013) considered the role of large-scale climatic indices like El Niño Southern Oscillation (ENSO) that promote increased surface mass loss due to reduced precipitation and increased air temperatures. However, poor correlations have also been reported between the ENSO and precipitation: based on 18 yr of data, Ramallo (2013) finds that the two variables have less than 10% of common variance at interannual scale on the Altiplano and less than 30% in the Zongo Valley.

In this context, distributed energy balance models (DEBAMs) are useful tools as they provide insight into the mechanisms that control interseasonal and interannual surface mass-balance variability of entire glaciers. Here, we focus on Zongo Glacier, located in the outer tropical Andes of Bolivia, where diverse long-term observations are available from previous studies.

Wagon et al. (1999) calculated the surface energy balance of Zongo Glacier at the automatic weather station (AWS) in the ablation area over one hydrological year (1997/1998). This was the first study of the annual surface energy balance over the glacier; it showed that the main driver of mass loss is the net all-wave radiation, which is primarily controlled by an albedo feedback effect. The authors also pointed out that because the meteorological conditions favor sublimation during the austral winter (between May and August, also known as the dry season) the melt rate over this period is lower than over the rest of the year, a process already identified by Kaser et al. (1990). Using data acquired between 1999 and 2000, Sicart et al. (2011) applied the physically-based DEBAM, (Hock & Holmgren, 2005) to the whole glacier in order to study the seasonal variability of the surface mass balance. This study highlighted the notable influence of processes that occur during the transition period between the dry (June–August) and wet season (January–March) on the annual surface mass balance. In addition, they show that at the glacier scale sublimation does not play an important role in controlling seasonal melt rate changes.

Lejeune et al. (2007) applied the CROCUS-ISBA model forced by meteorological data from an AWS on the moraine of Zongo Glacier. These authors showed that the rapid melting of snow on the moraine is mainly driven by incident shortwave radiation.

In this study, we applied DEBAM to Zongo Glacier over nine years to obtain deeper insights into the atmospheric/meteorological factors that control the interannual variability of the surface mass balance. The long data set available at Zongo Glacier provides a unique opportunity to investigate the climate factors that control both interannual and seasonal variabilities of the surface mass balance. Model experiments are performed to investigate the role of precipitation frequency and cloud cover on mass balance based on synthetic climate scenarios constructed from reorganized climate observations.

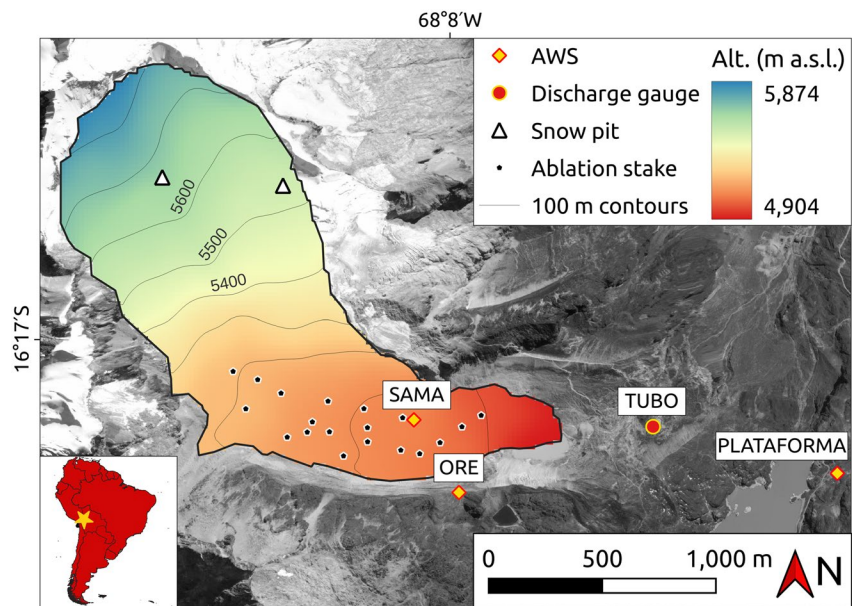


**Figure 1.** Location of Zongo Glacier and its monitoring network. SAMA is the on-glacier AWS, ORE is the AWS on the moraine and PLATAFORMA is the one at the pass. TUBO is a discharge gauging station. The bottom left inset map shows the location of the glacier in South America. The thick black line is the glacier outline in 1999. Thin black lines are elevation contours every 100 m from the 1999 digital elevation model (the first elevation contour being 5,000 m a.s.l.). The image in the background was acquired by the Pléiades satellite in 2013, © CNES–Airbus D&S.

## 2. Study Area and Climate Setting

### 2.1. Zongo Glacier

Zongo Glacier ( $16^{\circ}15'S$ ,  $68^{\circ}10'W$ ) is located on the southern side of Huayna Potosi peak (Cordillera Real, Bolivia). It is a valley-type glacier extending 2.8 km from about 6,000 m a.s.l. down to about 4,950 m a.s.l. and had a surface area of 1.7 km<sup>2</sup> in 2016. In collaboration with the French Research Institute IRD, the Bolivian authorities started a meteorological, glaciological, and hydrological observation program on Zongo Glacier in 1991 (Francou et al., 1995; Ribstein et al., 1995). The location of the AWS s on and around the glacier as well as the ablation stakes have varied over time but measurements have continued uninterrupted since the beginning of the program; see Rabatel et al. (2013) for a detailed overview of the monitoring network, and Figure S1 in Supporting Information S1 for the operating periods of the three AWS s. Figure 1 shows the location of the glacier along with its monitoring network.

### 2.2. Tropical Climate and Glaciological Regime

Since Zongo Glacier is located in the outer tropics, its climate is characterized by marked seasonality with frequent cloud cover and precipitation events primarily during the austral summer and a pronounced dry season during the austral winter (Troll, 1941). The glaciological regime over this region was described by Kaser (2001): most accumulation occurs during the wet season (austral summer) whereas during the dry season (austral winter) predominant clear-sky conditions and dry air favor sublimation. This overall pattern has been well established from in situ monitoring, for instance by Kaser et al. (1990) over glaciers in the Cordillera Blanca, Hardy et al. (1998) on Sajama Ice cap and by Wagnon et al. (1999) at Zongo Glacier. Sicart et al. (2011) found that the low ablation rate during the dry season is linked to the large longwave emission deficit during this period. Note that the hydrological year for Zongo Glacier begins in September and ends the following August.

We analyzed the mass-balance record (1992–2017, Vincent et al., 2018) to characterize the glaciological regime of the glacier. As shown in Figure 2, the ablation zone of Zongo Glacier experiences the highest net mass losses from September to November (−0.21 to −0.50 m w.e./month). This period is considered as the transition period

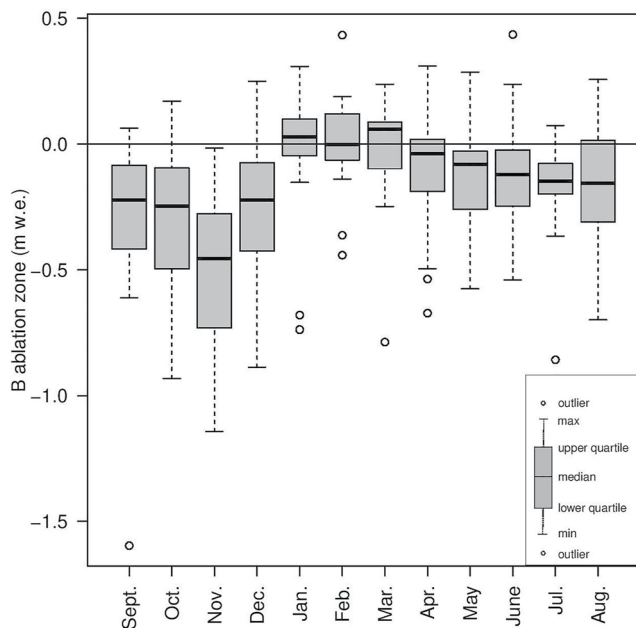


**Figure 2.** Box plot showing the monthly surface mass balances of the ablation zone of Zongo Glacier calculated from 20 ablation stakes (between 5,000 and 5,200 m a.s.l.) for the 27 mass balance years 1990/1991–2016/2017.

between the dry and the wet seasons. It is also characterized by very high interannual variability of the surface mass balance (standard deviation of 0.29 m w.e./month on average for the three months). Ramallo (2013) reported that about 20% of annual precipitation occurs during this period. Most cloud events during this period (80%, Sicart et al., 2016) are linked to northward propagating wind incursions to the east of the Cordillera (Surazos) that lead to deep convection events (Garreaud, 2000). Previous studies (e.g., Sicart et al., 2011) have shown that this period plays a key role in explaining the annual surface mass balance.

During the wet season (January–March), the surface mass balance in the ablation area is either slightly negative or positive. This period corresponds to the core of the wet season linked to the mature phase of the South American Monsoon System (SAMS). As the SAMS develops, the diabatic heating over the western Amazon leads to the formation of the anticyclonic system known as the Bolivian High in the upper troposphere (Lenters & Cook, 1997). Meanwhile, in the lower troposphere, the southward displacement of the South American Low-Level Jet favors mean easterly winds on the northern arc of the Bolivian High, which in turn, allow the formation of strong heat-driven easterly winds on the eastern slopes of the Cordillera Real. These upslope winds transport moisture from the Amazon Basin to the tropical Andes. The solar heating of the surface leads to strong afternoon/early evening convection events in the Bolivian Andes and Altiplano (Garreaud et al., 2003). According to Sicart et al. (2016), nearly half the cloud events during this period can be linked to Surazo conditions. These correspond to a destabilization of the tropical atmosphere by extra tropical cold air intrusion

related to low-level southern wind incursion (Ronchail, 1989). In the Bolivian lowlands, Espinoza et al. (2013) found an average of 3.4 such events lasting 2.7 days for each austral winter (JJA) between 1975 and 2002. Over this region, such events can cause sudden drops in temperature associated with deep convection events (Sicart et al., 2016). These events are responsible for up to a quarter of the summer precipitation in central Amazonia (Garreaud & Wallace, 1998). Over Zongo Glacier, they are marked by the arrival of cold high-altitude clouds which bring snow events which usually last for a few days. These events differ from the monsoon events which are convective events (i.e., thick and warm clouds) resulting from moist air advection from the Amazon Basin toward the eastern Andes due the destabilization of the boundary layer via the intense heating of the Altiplano between December and March (Sicart et al., 2016).

Throughout this period (wet season), there is little net mass loss since most of the melt energy goes to melting fresh snow (70% of the annual melt; Ramallo, 2013). Indeed, as shown by Sicart et al. (2011), throughout this season at the glacier snout, periods of snow melt during cloud events alternate with periods of ice melt during clear sky periods.

Finally, between April and August, surface mass-balance in the ablation area becomes increasingly negative, and both the top of atmosphere shortwave and incoming longwave radiation fluxes are low. The large incoming longwave deficit leaves little energy available for melt (Sicart et al., 2005). In addition, the negative latent heat fluxes during this period favor strong sublimation (Wagnon et al., 1999). About 10% of the annual precipitation occurs during this period (Ramallo, 2013), and 87% of the cloud events can be linked to Surazo conditions (Sicart et al., 2016).

While the top of atmosphere shortwave radiation peaks between September and November (Figure 3a), incoming shortwave radiation is at its maximum during the dry season (May–August). In contrast, the incoming longwave radiation is highest during the core wet season (January–March) and minimal during the dry season (Figure 3b). Sicart et al. (2010) showed that clouds increased the longwave radiation by up to 55% during the wet season and by about 20% on average. This effect contributes to the significant mass loss in the ablation area during the transition period (September–November, Figure 2).

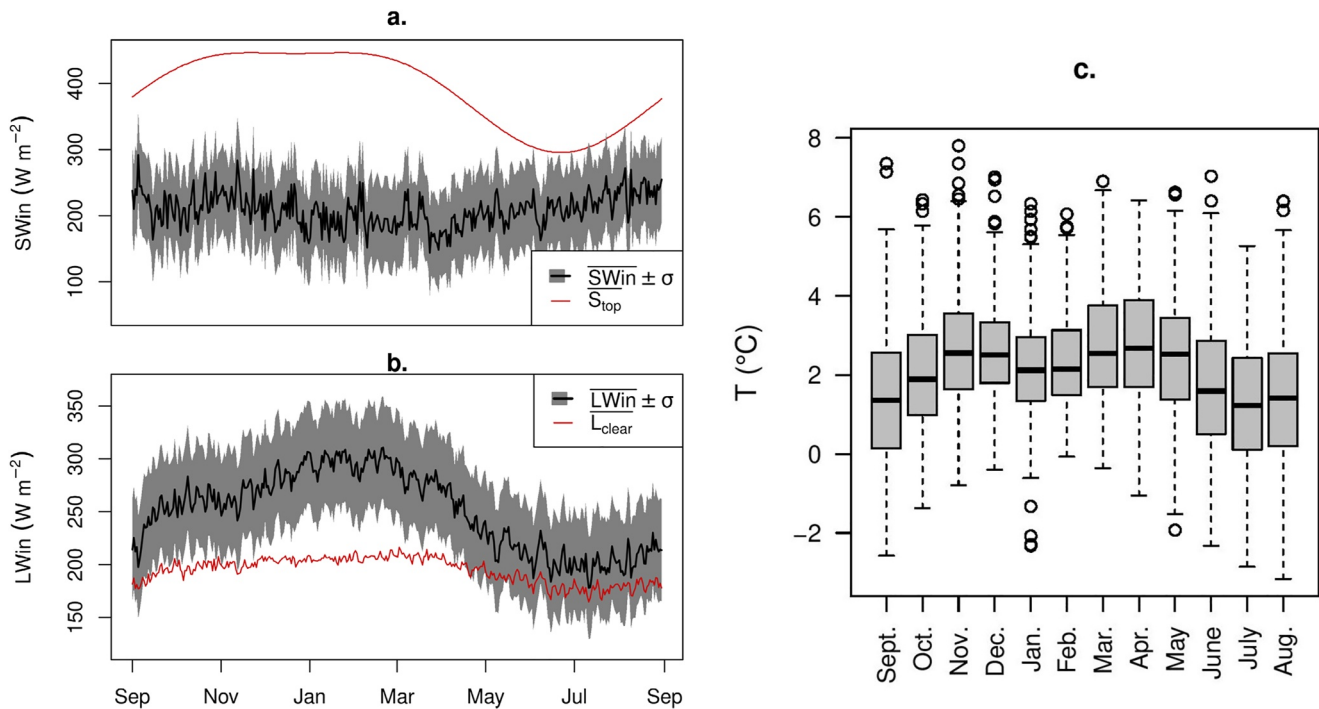


**Figure 3.** Annual cycle of (a) incoming shortwave radiation (SWin) and top of the atmosphere shortwave radiation ( $S_{top}$ ) and (b) incoming longwave radiation (LWin) at the on-glacier weather station (SAMA) and theoretical clear-sky incoming longwave radiation ( $L_{clear}$ ).  $L_{clear}$  was derived by dividing LWin by the cloud longwave emission factor ( $F$ ). Daily mean station data are averaged over the nine simulated years between 1999 and 2017. (c) Boxplot showing the interannual variability of the monthly mean near-surface air temperature at the PLATAFORMA weather station (Figure 1).

Both incoming short and longwave radiation fluxes (averaged over each mass-balance year) are rather poorly correlated with the annual surface mass balance ( $R^2 = 0.28$  and  $0.0$ , respectively) for the nine study years.

Figure 3c shows the interannual variability of the monthly mean temperatures at PLATAFORMA over a period of 14 yr (between 1999 and 2017): as expected the seasonal variability of the monthly average is low (the median temperatures vary between  $1.5^{\circ}C$  and  $2.2^{\circ}C$ ). We correlated monthly mass balances to monthly mean air temperatures at the on-glacier weather station (SAMA) and found the best correlation during the core wet season (up to  $R^2 = 0.69$ ). The best correlations with glacier-wide surface mass balance derived from extrapolating the point balances across the glacier using a nonlinear statistical model (Vincent et al., 2018) were obtained at the annual scale but remained low ( $R^2 = 0.18$ ).

Seasons can also be defined by looking at the distribution of the cloud radiative properties and more specifically at cloud radiative forcing, that is, the combined effect of clouds on the incoming radiation fluxes resulting from an increase in longwave radiation and a reduction in incoming shortwave radiation, the latter being dominant. Following the methodology of Sicart et al. (2016), we calculated the cloud radiative forcing of cloudy days for each month of 13 yr between 1999 and 2017, and analyzed the monthly probability density functions (Figure 4). Results indicate that cloud radiative forcing is distinctly different for the core wet season (January–March), the dry season (June–August) and the transition period (September–November), and therefore can be used as a criterion to identify these three seasons.

Between September and November (transition period, Figure 4a), the bimodal distribution of the cloud radiative forcing suggests the presence of two different types of clouds: those with little impact on the radiation budget (cold high-altitude thin clouds), and clouds with a considerable impact on the radiative budget as evidenced by the peak around  $-120 W m^{-2}$ ; that is, thick clouds typical of convective events. During the core wet season (January–March, Figure 4b) the cloud distribution is unimodal, and the peak is centered around  $-150 W m^{-2}$ , suggesting predominantly thick clouds. Finally, the distribution is again unimodal during the dry season, centered around  $-20 W m^{-2}$ , indicating predominantly thin clouds at high altitude with a small impact on the radiation budget.

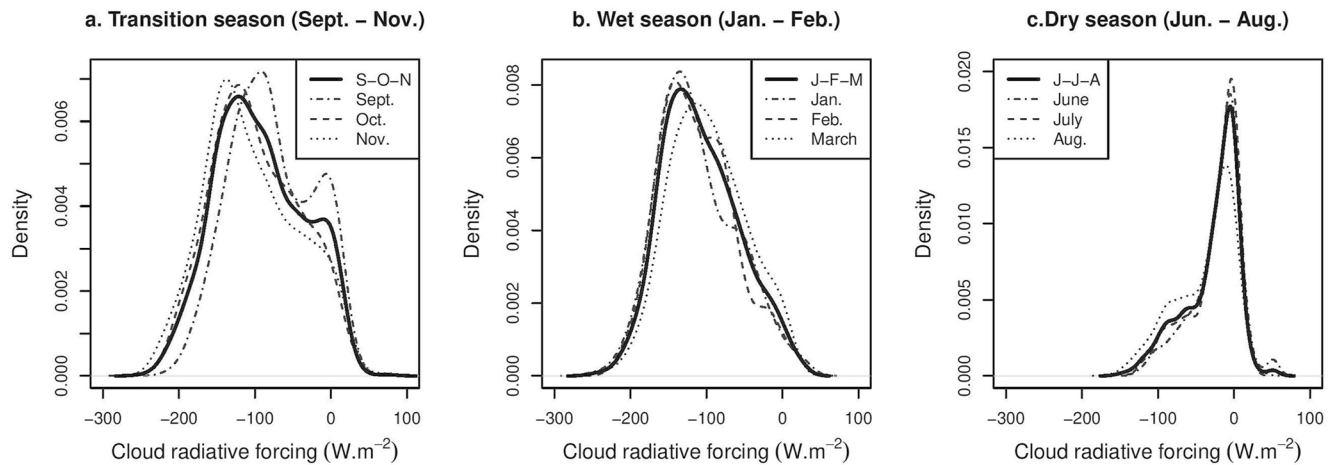


**Figure 4.** Probability distribution functions of cloud radiative forcing for the transition period (a), the core wet season (b) and the dry season (c) based on 13 yr of data (between 1999 and 2017) at both the on-glacier and PLATAFORMA weather stations.

### 3. Mass-Balance Modeling

We apply the open-source mass-balance model DEBAM (Hock & Holmgren, 2005; <https://regine.github.io/melt-model/>) to nine non-consecutive years between 1999 and 2017 when weather station data were available to reliably simulate the energy and mass fluxes over the glacier surface at the hourly time step. Although less complex than other physically based models (e.g., CROCUS-ISBA), DEBAM requires less meteorological input variables, and therefore is well suited to study the interannual variability of Zongo Glacier surface mass balance. This model has been applied to glaciers in the Northern Hemisphere (Hock & Holmgren, 2005; Østby et al., 2017; Reijmer & Hock, 2008), the Sub-Antarctic (Braun & Hock, 2004) and on Zongo Glacier (Sicart, 2002; Sicart et al., 2011).

#### 3.1. Input Data Sets

The model is forced with seven meteorological input variables at hourly resolution: air temperature, precipitation, incoming shortwave and longwave radiation, outgoing longwave radiation, relative humidity, and wind speed. Due to the difficulty of maintaining a fully operational AWS on the glacier, sufficient data were only available for nine non-consecutive years within an 18 yr period from 1999 to 2017: 1999 to 2001, 2004 to 2006, 2008 to 2010, 2011 to 2013, and 2016/2017.

We use the data from the SAMA AWS located on the glacier surface at 5,050 m a.s.l (Figure 1, Table 1). Text S1 in Supporting Information S1 details the gap-filling methodology used.

**Table 1**  
*List of the Equipment at SAMA Along With the Sensor Heights and Precision According to the Manufacturer*

Variable	Sensor	Sensor height	Precision (according to the manufacturer)
Temperature	CS2115 (since 23/02/2011)	1.00 m	±0.2°C
	Vaisala HMP45C (up to 23/02/2011)	1.57 m	±0.9°C
Relative humidity	CS2115 (since 23/02/2011)	1.00 m	±2%
	Vaisala HMP45C (up to 23/02/2011)	1.57 m	±4%
Wind speed (m/s)	Gill Solent (since 23/02/2011)	1.74 m	±5%
	Young 05103 (up to 23/02/2011)	2.50 m	±0.3 m/s
Incoming and outgoing shortwave radiation (W/m <sup>2</sup> )	Kipp & Zonen CM3 0,305 < λ < 2,8 μm	1.00 m	±3%
Incoming and outgoing longwave radiation (W/m <sup>2</sup> )	Kipp & Zonen CG3 5 < λ < 50 μm	1.00 m	±3%
Snow height, ultrasonic measurements	Campbell, SR50AT	1.15 m	±1 cm or 0.4% of the distance

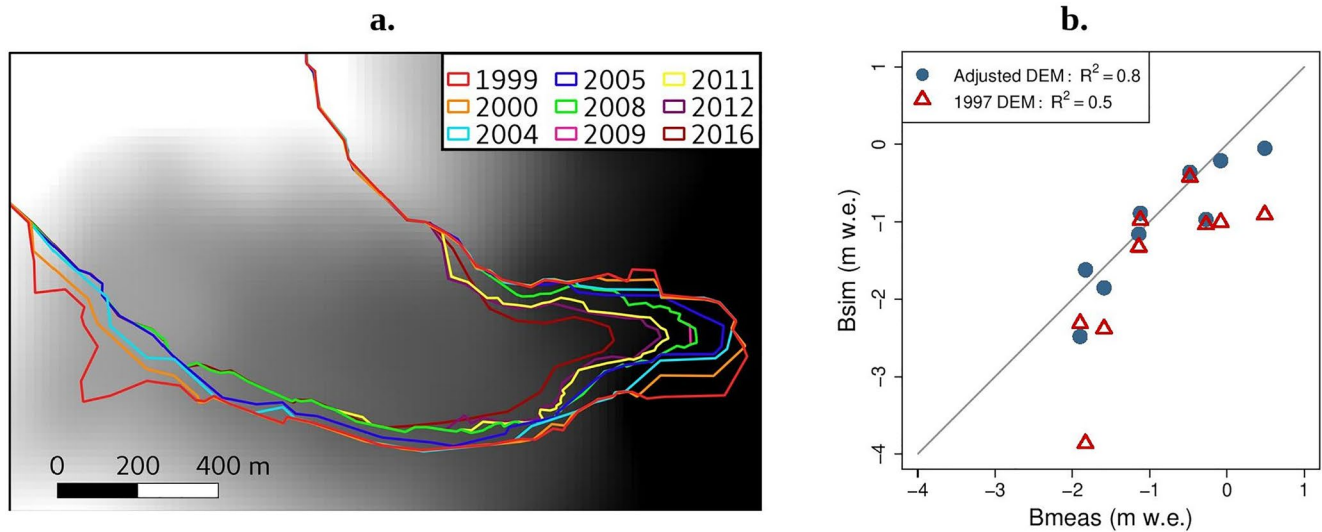


**Figure 5.** (a) Zongo glacier front positions between the first (1999) and the last modeled year (2016). (b) Simulated glacier-wide annual surface mass balance ( $B_{sim}$ ) vs. balances derived from stake observations and geodetic balances ( $B_{meas}$ , Vincent et al., 2018), including the 1:1 line. Simulations using annually adjusted DEMs are compared to those keeping the 1997 DEM and outline constant.

Precipitation was derived from the ultrasonic gauge measurements following Sicart et al. (2002): precipitation amounts were obtained by comparing the means of three consecutive measurements spread over one hour at 3 hr intervals, in order to identify changes in surface height of at least 1 cm. The amounts in water equivalent were then derived by applying a fresh snow density of  $220 \text{ kg m}^{-3}$  for the transition period and the dry season and a higher density of  $250 \text{ kg m}^{-3}$  for the wet season due to slightly higher temperatures during the austral summer.

Between 1999 and 2016, the glacier lost 12% of its surface area (Figure 5a) and thinned considerably (the altitude of the grid points making up the glacier front in 2016 were 55 m lower in 2016 than in 1999). To account for the changing geometry, digital elevation models (DEMs) were generated for each modeled year. The glacier topography was interpolated (or extrapolated) linearly between two measured DEMs: one from 1997 based on aerial photographs (Soruco et al., 2009) and one from 2013 made from Pléiades satellite stereo-images (Cusicanqui et al., 2015). The glacier contours were based on differential GPS measurements made each year during field campaigns.

Figure 5a illustrates the glacier retreat during the modeled period while plot 5b shows the impact of accounting for changing surface elevations compared to the use of the 1997 DEM on the simulated annual surface mass balance ( $B_{meas}$ , Vincent et al., 2018). Accounting for the glacier retreat improved the correlation between the simulated glacier-wide annual surface mass balances and those derived from observations ( $R^2$  went from 0.5 to 0.84). This is because accounting for glacier retreat adjusts the size of the ablation zone thereby significantly reducing the overall melt.

In addition, when keeping the glacier topography constant, the simulated snowline is at a higher altitude than what observations indicate. Therefore, simulated glacier-wide albedo is too low which in turn increases both melt and total mass loss.

Hourly discharge data from the TUBO gauging station (Figure 1), a V-shaped weir with an automatic limnigraph, were used for validation as it is representative of the overall amount of melt water. In addition, surface mass balance observations at 20 ablation stakes distributed over the ablation area were used. Finally, photos taken during field campaigns were used to compare the modeled and observed snow line positions.

### 3.2. Model Description

DEBAM (Hock & Holmgren, 2005) solves the following surface energy balance equation:

$$Q_M = G(1 - \alpha) + LW_{net} + H + LE + Q_G + R \quad (1)$$



where  $Q_M$  is the energy available for melt,  $G$  is the global (or shortwave incoming,  $SW_{in}$ ) radiation,  $\alpha$  the albedo,  $LW_{net}$  the net longwave radiation balance,  $H$  and  $LE$  are the sensible and latent heat fluxes, respectively,  $Q_G$  is the ground heat flux and  $R$  the sensible heat supplied by rain (negligible over Zongo as shown by Sicart et al., 2011). The model convention is such that energy fluxes directed toward the surface are positive and those away from the surface are negative.

The model also includes a runoff module which routes glacier melt and rain water through the glacier using three linear reservoirs representing firn, snow and ice. We use storage constants of 350, 30, and 16 hr, respectively, according to Sicart et al. (2011).

### 3.2.1. Incoming Radiation Fluxes

To extrapolate global radiation across the glacier, measured radiation was split into its direct and diffuse components using a calibrated empirical relationship between the ratio of global radiation at the top of the atmosphere and the potential diffuse radiation considering a clear sky attenuation of 13% at the daily time scale (Sicart et al., 2011). The diffuse radiation component was considered to be spatially variable and extrapolated according to topographic shading based on the sun's path, the effective horizon and sky view factor of the grid cell (Hock, 1998). The direct component of incoming shortwave radiation was extrapolated according to the slope and orientation of the grid cells. The incoming longwave radiation was taken from the weather station measurements and assumed to be spatially constant over the glacier, a reasonable assumption given the small glacier surface area (1.7 km<sup>2</sup>).

### 3.2.2. Parameterization of Albedo

Because DEBAM was originally developed to model glaciers in the Northern Hemisphere, a key adaptation to tropical glacier on the albedo calculation was implemented in the model by Sicart (2002), and was used here. It consists of a modified version of Oerlemans and Knap (1998)'s albedo parameterization that accounts for the rapid alternation of accumulation and melt in the wet season as well as the impact of ice on the albedo over shallow snow depths.

In the absence of precipitation, the snow albedo decreases as follows:

$$\alpha_{\text{snow}} = \alpha_{\text{firn}} + (\alpha_{\text{fresh-snow}} - \alpha_{\text{firn}}) e^{-nj/n^*} \quad (2)$$

$$\alpha = \alpha_{\text{snow}} + (\alpha_{\text{ice}} - \alpha_{\text{snow}}) (1 + e_s/e_s^*)^{-3} \quad (3)$$

where  $n^*$  is the time constant of decrease in albedo (10 days),  $nj$  is the number of days since the last snowfall,  $e_s$  the snow depth and  $e_s^*$  the critical snow depth below which the ice starts to influence the modeled albedo, considered here to be 6 mm w.e. according to Sicart (2002).

During precipitation events, the albedo increases proportionally to precipitation rate ( $Pr$ ) (Sicart, 2002):

$$\Delta\alpha = cpPr \text{ with } cp = 0.02 \text{ h/mm} \quad (4)$$

### 3.2.3. Surface Temperature

Surface temperature was derived from measured outgoing longwave radiation and assumed constant across the glacier. The subsurface snow module (Hock & Tijn-Reijmer, 2012) was not used to evaluate the surface temperature spatial evolution due to lack of data to constrain the model (i.e., subsurface temperature and density profiles). In addition, most of the melt occurs between September and March when the surface temperatures in the ablation area remain close to the melting point (Sicart et al., 2011). Thus its application would significantly increase the model uncertainty and hence the risk of error compensation.

### 3.2.4. Turbulent Energy Fluxes

The sensible and latent turbulent heat fluxes were calculated according to the aerodynamic profile method between the glacier surface and measurements as a function of 1.57 m air temperature, relative humidity, and wind speed based on the Monin-Obukhov similarity theory (see Hock & Holmgren, 2005 for more details). Stability functions were assumed constant across the glacier and based on Beljaars and Holtslag (1991) for stable conditions and on the Businger-Dyer expressions from Paulson (1970) for the less frequent unstable cases.

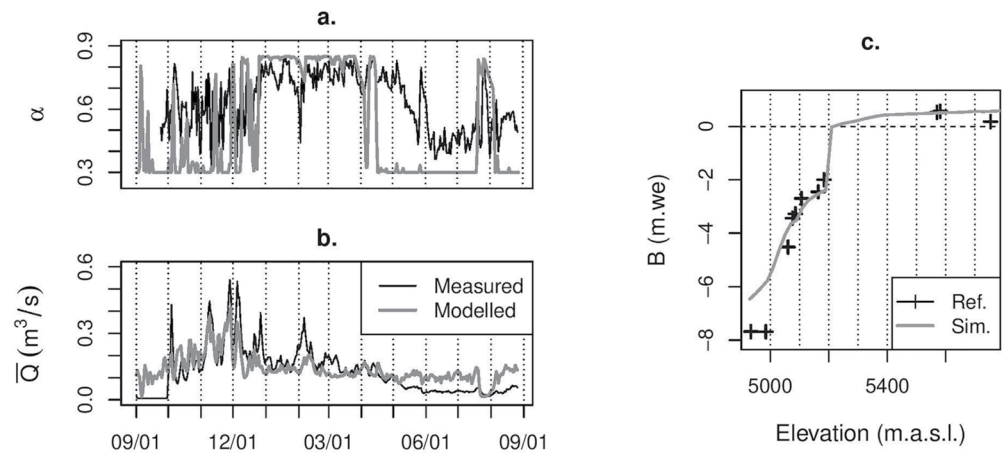


**Figure 6.** Validation of the model results exemplified for the hydrological year 2008/2009. Modeled and measured (a) daily mean albedo ( $\alpha$ ), (b) daily discharge ( $Q$ ) and (c) annual specific surface mass balance ( $B$ ) profiles.

### 3.2.5. Model Application and Calibration

The model was run with hourly resolution and on a  $20 \times 20$  m grid. Air temperature was extrapolated across the glacier using a constant lapse rate of  $-0.55$  K/100 m. A precipitation gradient of  $+10\%/100$  m was applied up to 5,400 m a.s.l., above which it remained constant (based on an analysis of measurements at different altitudes). Relative humidity and wind speed were assumed constant across the glacier. At the beginning of each hydrological year (1 September), the model was initialized with a map of the extent of the firn zone estimated from in situ terrestrial photographs or LANDSAT images and a map of snow cover derived from field photographs, and snow depth derived from observations.

First, the melt rate was calculated at the AWS. The energy fluxes were then extrapolated across the glacier.

We chose to use a constant set of parameters for the nine years to guarantee robust calibration, the calibration process involved a trade-off between very precise modeling of specific years (e.g., years with high precipitation) and obtaining a globally efficient parameter set. Special emphasis was placed on reproducing the transition periods as accurately as possible as they play an important role in the interannual variability of the surface mass balance (Sicart et al., 2011). We focused on two main sets of parameters: albedo and roughness lengths.

The albedo was calibrated using measurements at SAMA for two contrasting years (1999/2000,  $B = -0.08$  m w.e. and 2004/2005,  $B = -1.90$  m w.e.). It implied a trade-off between the simulated albedo for these two years. It was validated over the remaining years. Accordingly, the following albedo values were assumed: 0.85 for fresh snow, 0.6 for firn and 0.3 for ice.

The roughness length for momentum over ice was calibrated using eddy covariance (EC) measurements in June 2011 and set to 0.026 m. Those of momentum over snow and of temperature and humidity were considered constant and set to a tenth of the roughness length of momentum over ice (i.e., 0.0026 m). These values were then validated over the other period where EC measurements were available (July–August 2007, Litt et al., 2014).

### 3.3. Model Validation

To validate model performances, we focus on the following observations: albedo at SAMA, discharge at TUBO gauging station, observations of surface type (snow, ice) from terrestrial photographs, glacier-wide surface mass balances derived from observations, and point surface mass balances as a function of altitude.

Figure 6 illustrates the results for the year 2008/2009, a year with high albedo variability at the AWS. Overall, variations in albedo are well simulated but the amplitude is sometimes off (Figure 6a), suggesting that precipitation events are well represented, but not always their intensity. This is due to both the precipitation measurements uncertainties (Sicart et al., 2002) and the assumption of a constant value for the time constant of decrease in albedo (10 days, Equation 2) although snow ages faster in the wet season than in the dry season (Sicart et al., 2011).

Errors in modeled albedo have a significant impact on modeled melt rate, since solar irradiance is often the main source of energy for melt (Sicart et al., 2005) and its effect on melt is controlled via an albedo feedback effect (and hence the glacier surface state). In addition, errors in simulated surface state lead to erroneous turbulent flux simulations as different roughness lengths are used over snow and ice.

Simulated discharge is in good agreement with the measurements up to the end of the wet season (Figure 6b) although the model underestimates some peaks probably due to errors in accurately modeling the snow line on a daily scale. During the dry season, the discharge is systematically overestimated likely because the model does not account for the ground heat flux. Hence, the glacier surface does not cool enough and cannot delay the diurnal melt.

Figure 6c compares modeled and observed surface mass-balance as a function of altitude. The model underestimates mass loss close to the glacier front however, this has little impact on the glacier-wide surface mass balance since this region represents only a very small fraction of the ablation area. The mass balance for the remaining glacier area is well simulated.

Measured and simulated surface mass balance profiles for all nine simulated years are shown in Figure S2 in Supporting Information S1. Overall, the simulated equilibrium-line altitude is in good agreement with the measurements.

One of the main drawbacks of calibrating a single parameter set for all the modeled years is that the model is not equally accurate for each of the years modeled: in some years, melt in the ablation zone is underestimated (e.g., 2005/2006) whereas in others, it is overestimated (e.g., 2004/2005). Considering the nine-year average, the overall mass loss is overestimated by 0.18 m w.e. with an average surface mass balance of  $-0.88$  m w.e. The simulation errors for years with significant net mass loss tend to be higher than for years with limited mass loss.

Overall, a variety of error sources can explain the differences between measured and simulated variables (Sicart et al., 2011). In the model, the surface temperature is calculated using the measured outgoing longwave radiation at the weather station and considered constant. As a result, the model is not able to capture the intense night cooling of the surface in the firn area, which in turn, delays the diurnal melting period of the surface, leading to potential overestimation of the melt rate. Furthermore, erroneous surface temperatures affect the simulated turbulent fluxes which in turn, affect the surface temperature, leading to rapid uncertainty propagation. This process is particularly important in the dry season when nighttime cooling of the surface in the accumulation area is at its highest.

### 3.4. Generation of Scenarios for Precipitation Sensitivity Analysis

We perform a series of sensitivity experiments to analyze the impact of the timing of precipitation amounts during the transition season (September–November) on the annual surface mass balance. Three scenarios (S1–S3) were generated by shuffling the time series of daily meteorological data during the transition season:

1. S1: All days with precipitation events  $\geq 2$  mm/d were evenly distributed in time. For example, if there are 30 such days, then, in the scenario, such a day occurred every third day as there are 91 days in the season. Days were shuffled manually so that each day was moved as little as possible (maximum was 12 days). The threshold was chosen because it allows the formation of at least 1 cm of snow, which in turn, enables considerable changes in albedo and hence has a notable impact on the melt rate
2. S2: Same as S1 except the threshold was 9 mm/d (to assess the threshold impact)
3. S3: All precipitation events exceeding 2 mm/d within a given month were moved to the beginning of that month

The procedure guarantees that precipitation amounts in the transition period are conserved (i.e., only the temporal distribution of the events changes).

To guarantee physical coherence between the different meteorological variables for each day, all the other meteorological input data for the corresponding day were shuffled as well.

**Table 2**

Summary of the 66th Percentile Value of the Cloud Radiative Forcing (CF) Per Month and the Corresponding Cloud Longwave Emission Factor ( $F^{\text{cloud}}$ ) and Bulk Cloud Shortwave Transmissivity ( $Tn^{\text{cloud}}$ ) Values Retained for the Scenario

Month	66th percentile value of CF ( $\text{W m}^{-2}$ )	$F^{\text{cloud}}$	$Tn^{\text{cloud}}$
September	−109	1.42	0.47
October	−128	1.30	0.51
November	−136	1.23	0.53

Scenarios S1–S3 were generated for three contrasting years: 1999/2000 represents a year with little melt ( $B_{\text{meas}} = -0.08$  m w.e.), 2008/2009 represents a mass balance close to the nine-year average ( $B_{\text{meas}} = -1.14$  m w.e.). The year 2004/2005 had the highest recorded net mass loss of the nine years studied ( $B_{\text{meas}} = -1.90$  m w.e.).

Moving days around also impacts the daily total incoming radiation at the glacier surface via cloud radiative forcing as moving precipitation events also involve displacing clouds. But, as melt was generally limited during precipitation events, the cloud radiative forcing induced by moving the clouds was of little importance.

### 3.5. Generation of Scenarios for Cloud Sensitivity Analysis

To assess the impact of the cloud cover on the annual surface mass balance, we constructed three scenarios that change the cloud radiative forcing (which is the net effect of clouds on the incoming radiation fluxes) to mimic a cloud cover sustained over an entire month. In practice, we changed the incoming shortwave and longwave radiation for each time step, separately for each of the three months of the transition period (September–November) for all nine simulated years resulting in three scenarios: Sce\_S, Sce\_O, and Sce\_N. The radiative forcing of all other months and all other meteorological data for the entire period remained unaltered.

To achieve this we used the cloud emission factor  $F$  which represents the increase in sky longwave emission due to clouds and the bulk cloud shortwave transmissivity  $Tn$  which represents the attenuation of incoming shortwave radiation linked to the presence of clouds (Sicart et al., 2010, 2016).

Thus, the incoming longwave radiation flux in each scenario ( $LW_{\text{in}}^{\text{Sce}}$ ) was calculated by:

$$LW_{\text{in}}^{\text{Sce}} = (F^{\text{cloud}}/F^{\text{meas}}) LW_{\text{in}}^{\text{meas}} \quad (5)$$

where  $LW_{\text{in}}$  is the measured longwave incoming radiation,  $F^{\text{meas}}$  is the measured cloud emission factor and  $F^{\text{cloud}}$  is the emission factor needed to construct the scenario.

Similarly, the incoming shortwave radiation ( $SW_{\text{in}}^{\text{Sce}}$ ) was calculated by scaling measured  $SW_{\text{in}}^{\text{meas}}$  by the ratio of the bulk shortwave transmissivity representing cloudy conditions ( $Tn^{\text{cloud}}$ ) and the measured transmissivity ( $Tn^{\text{meas}}$ ):

$$SW_{\text{in}}^{\text{Sce}} = (Tn^{\text{cloud}}/Tn^{\text{meas}}) SW_{\text{in}}^{\text{meas}} \quad (6)$$

$F^{\text{cloud}}$  and  $Tn^{\text{cloud}}$  were derived from the long-term (nine-year) monthly 66th percentile of cloud radiative forcing. We assume that the 66th percentile of daily values over the nine simulated years represents thick cloud cover. Table 2 lists the cloud radiative properties for each month. The  $F$  and  $Tn$  values are typical of thick warm clouds: regardless of the month considered, the clouds reduce the incoming shortwave radiation by at least 47% and increase the incoming longwave radiation by at least 23% (Sicart et al., 2016 considered that clouds have a strong impact on the radiative budget when  $F \geq 1.15$ ).

Although changing the incoming radiation fluxes values led to a loss of physical coherence between radiation fluxes and the other meteorological variables (temperature, relative humidity, and wind speed), the loss was considered acceptable since the main impact is on the turbulent fluxes which, according to Sicart et al. (2011), tend to be small during the transition period.

In order to assess the impact of generating the cloud cover scenarios compared to measured conditions, the mean number of cloud events per month over 13 yr was calculated based on the methodology defined in Sicart et al. (2016). Accordingly, there were 20 cloudy days in September, 25 in October, and 24 in November. Hence, on average the scenarios implied adding 10 cloudy days in September and six cloudy days in both October and November.

It is worth noting that the cloud radiative forcing values applied were significantly lower than the measured values: for each month, the mean cloud radiative forcing was 34% more negative than the nine-year average (as the 66th

**Table 3**

*Simulated Annual Glacier-Wide Surface Mass Balance, Melt and Precipitation in the Nine Simulated Years, Along With the Differences From Their Respective Mean Values*

Years	Simulated variable X			Difference from mean values ( $X - \bar{X}$ )		
	B (m w.e.)	Melt (m w.e.)	Precipitation (m)	B (m w.e.)	Melt (m w.e.)	Precipitation (m)
<i>1999/2000</i>	-0.21	1.93	1.74	0.85	-0.64	0.13
<i>2000/2001</i>	-0.04	2.03	1.98	1.02	-0.53	0.37
<b>2004/2005</b>	-2.47	3.49	1.35	-1.41	0.93	-0.26
<i>2005/2006</i>	-0.36	2.25	1.91	0.70	-0.32	0.31
<i>2008/2009</i>	-1.14	2.38	1.41	-0.08	-0.19	-0.20
<b>2009/2010</b>	-1.84	3.00	1.47	-0.79	0.43	-0.14
<i>2011/2012</i>	-0.88	2.55	1.76	0.18	-0.01	0.15
<i>2012/2013</i>	-0.97	2.51	1.53	0.09	-0.06	-0.80
<b>2016/2017</b>	-1.62	2.96	1.32	-0.56	0.39	-0.29
$\bar{X}$	-1.06	2.60	1.61	NA	NA	NA
$\sigma$	0.81	0.50	0.25	0.81	0.50	0.25

*Note.* The three years in italics are years in which the mass loss is considerably less than the average ( $B > B_{\text{mean}} + \sigma/2$ ). The three years in bold are years with considerable mass loss ( $B < B_{\text{mean}} - \sigma/2$ ).

percentile of the absolute cloud radiative forcing was used to build the scenarios). In terms of intrinsic cloud radiative properties, this increased the cloud longwave emission factor ( $F$ ) by 12%, 1%, and 6% in the September, October, and November scenarios, respectively. Similarly, it reduced bulk cloud shortwave transmissivity ( $Tn$ ) by 33%, 14%, and 9% in September, October, and November, respectively. Therefore, this scenario generation method allows the assessment of the impact of strong sustained cloud cover on the surface mass balance.

## 4. Results and Discussion

### 4.1. Analysis of the Interannual Variability of the Simulated Energy Fluxes

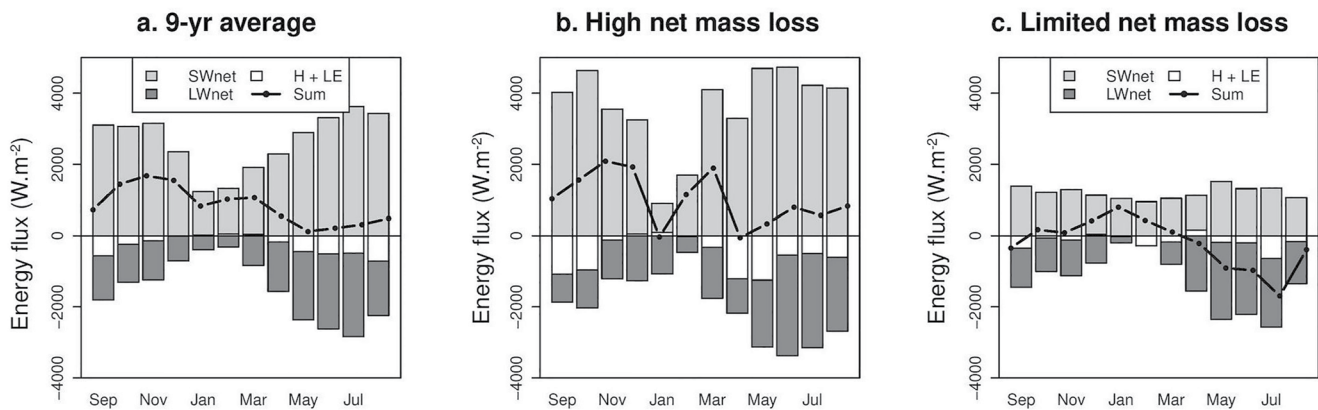
Simulated annual glacier-wide surface mass balances range between 0.49 and  $-1.90$  m w.e. indicating contrasting climate conditions between the nine simulated years. The average annual balance is strongly negative ( $-0.88$  m w.e.) suggesting that the glacier is not at equilibrium with climate.

Table 3 shows the modeled annual surface mass balance, melt, precipitation and their differences to the nine-year average. Years with limited net mass loss are years when the precipitation amounts were well above average ( $P > P_{\text{mean}} + \sigma/2$ ). Similarly, years with high net mass losses were years with a precipitation deficit ( $P < P_{\text{mean}} - \sigma/2$ ).

The monthly mean energy fluxes at the automatic weather station (SAMA) averaged over all nine years and for two contrasting years are presented in Figure 7. The AWS fluxes are presented rather than glacier-wide average fluxes in order to avoid simulation errors that are due to spatial extrapolation (e.g., temperature and precipitation gradients).

On average the sum of radiative and turbulent fluxes is lower during the dry season (June–August, Figure 7a). During this period, net longwave radiation deficit is greatest due to the absence of longwave radiation emitting clouds (Sicart et al., 2011). Conversely, during the transition period, the increase in surface temperatures combined with the increased frequency of cloud events and the increase in incoming solar radiation combined with a relatively low albedo result in large amounts of energy available for melt.

Figure 7b shows that much more energy is available for melt in the strongly negative mass-balance year. This is due to a significantly higher shortwave energy budget, while the longwave budget is less different than the long-term average.



**Figure 7.** Monthly mean energy fluxes (a) averaged over the nine simulated years, (b) for a year with a highly negative surface mass balance (2016/2017,  $-1.62$  m w.e.) and (c) for a year with limited net mass loss (1999/2000,  $-0.21$  m w.e.). The cumulative energy fluxes shown are the simulated fluxes at the automatic weather station (SAMA). Note, a positive sum implies that energy is available for melt, whereas a negative one implies surface cooling via the ground heat flux.

For a year with a limited net mass loss (Figure 7c), some energy was available for melt during the wet season, but the sum of the radiative and turbulent fluxes was mostly negative, resulting in surface cooling rather than melting. The differences to the long-term average are mainly explained by a lower net shortwave radiation budget due to a higher glacier-wide albedo.

Overall Figure 7 illustrates that the transition period controlled most of the annual surface mass balance as, both on average and for the year with significant mass loss, the transition period is when most energy is available for melt. When the sum of the energy fluxes is negative or close to zero during this period, the annual net mass loss is significantly lower than average (Figure 7c).

To better understand the interannual variability of the surface mass balance, three years with limited net mass loss: 1999/2000, 2000/2001, and 2005/2006 were compared to three years with high mass loss: 2004/2005, 2009/2010, and 2016/2017 (Table 3).

Results (illustrated for two contrasting years in Figure 8) show that during the transition period, years with limited mass loss systematically had a higher glacier-wide albedo (Figure 8a). This trend was sometimes inverted between March and May. At the annual scale, the mean annual albedo of the three years with limited melt was 13% higher than the mean for the three years with significant melt. During the transition period, it was 11% higher, while during the dry season it was 30% higher. However, during the core wet season, it was only 1% higher, this small difference is due to the frequent precipitation events during this period regardless of the year considered.

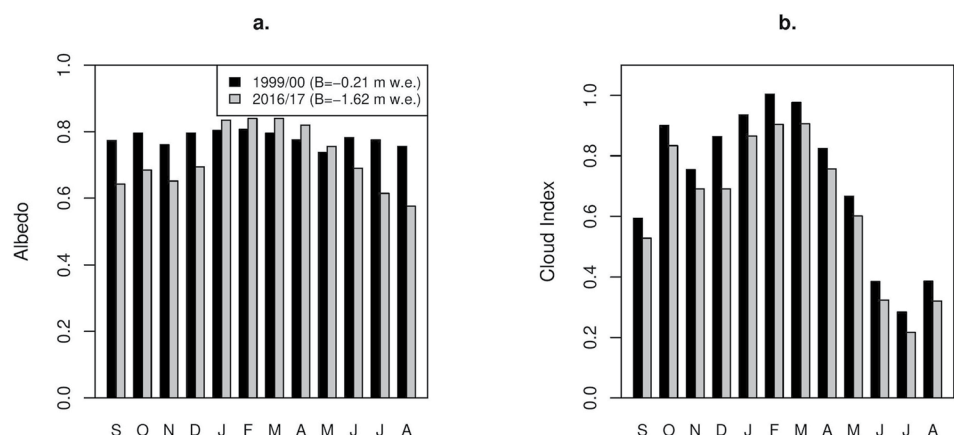


**Figure 8.** (a) Modeled monthly mean glacier-wide albedo ( $\alpha$ ), and (b) monthly mean cloud index (CI) for both a year with limited net mass loss (1999/2000;  $B = -0.21$  m w.e.) and a year with high net mass loss (2016/2017;  $B = -1.62$  m w.e.).

In addition, years with a significant mass loss tended to be less cloudy than years with a limited mass loss (Figure 8b). This is quantified by the mean monthly cloud cover index (CI) defined by Sicart et al. (2016) which is the difference between the cloud longwave emission factor and the bulk cloud shortwave transmissivity factor. The higher the index, the greater the ability of the clouds to reduce incoming solar radiation and increase incoming longwave radiation as. At the annual scale, the mean CI of the three years with limited mass loss was 15% higher than for years with significant mass loss, and at least 6% higher regardless of the season considered.

During the transition period, melt is highest during clear sky days (CI close to 0) as clouds reduce the amount of incoming energy at the surface. This coupled to the gradually increasing top of atmosphere radiation (as the summer solstice approaches) and the limited number of cloud events throughout the period make the albedo a key variable in controlling melt energy (via a feedback effect). Indeed, although the annual mass balance is poorly correlated with the incoming shortwave radiation ( $R^2 = 0.28$  when considering the nine years), it is well correlated with net shortwave radiation ( $R^2 = 0.84$ ) which highlights the importance of the albedo in the energy budget. Thus, despite observed similar differences in mean glacier-wide albedo and CI between years with low and high mass loss (Figure 8), it is the albedo that has the highest impact on melt energy.

This analysis shows that the transition period is most important in terms of controlling the interannual variability of the surface mass balance mainly because solar radiation approaches its maximum while cloud events are still sporadic, meaning it has the highest net incoming radiation. Coupled with the fact that during the transition period, the surface temperature in the ablation zone is close to 0°C, which limits the magnitude of the ground heat flux. As a result, most of the excess energy in the energy balance is converted into melt.

Finally, in order to assess if the mass balance deficit occurring during the transition season was persistent across the year, we carried out model runs where the data of the transition season of a year with limited mass loss (e.g., 2005/2006) was replaced by the data from another year with significant mass loss (e.g., 2004/2005) and vice-versa. The simulations show that the mass balance generated by the transition season is repercutated throughout the year. For example, when the year 2004/2005 is run with the transition season of 2005/2006, the annual simulated mass loss is reduced by 1.18 m w.e. Similarly, when 2005/2006 is run with the 2004/2005 transition season, the simulated annual net mass loss is increased by 1.00 m w.e.

## 4.2. Sensitivity to Precipitation Scenarios

### 4.2.1. Application to Three Contrasting Years

Figure 9 shows some impacts of the three scenarios over the 2008/2009 transition period. Overall patterns are similar for years with high and limited mass balances (not shown).

Evenly redistributing the precipitation events (S1 and S2) maintained a larger snow-covered area (Figure 9a) throughout most of the transition period, as also indicated by a generally higher albedo (Figure 9b), and hence a lower net shortwave radiation balance (Figure 9c), which in turn, resulted in a lower melt rate (Figure 9d). Averaged over the three years to which the scenarios were applied, scenarios S1 and S2 reduced the melt rate by 7% and 2%, respectively, whilst scenario S3 increased the melt rate by 12% over the transition period. Note that because scenario S1 involved moving more precipitation events than scenario S2, it reduced the melt rate more than the latter (as it maintained a larger glacier fresh snow cover).

In contrast, with scenario S3, grouping all the precipitation events at the beginning of the month yielded a much thicker snow cover at the beginning of the month (except in September 2008, due to a small amount of measured precipitation: 29 mm w.e.). However, due to a lack of precipitation for the rest of the month, this snow cover disappeared, resulting in a lower albedo than in the reference run, and thus, over the whole period, to larger amounts of energy available for melt.

Impacts of each scenario on the surface mass balance are shown in Figure S3 in Supporting Information S1 and Table 4 lists the precipitation amounts, simulated surface mass balances for scenario S1 and the reference run over the transition period.

Scenario S1 resulted in a smaller net mass loss over the transition period than the reference run in all years while scenarios S2 and S3 resulted in higher or lower net mass loss depending on the year. Overall, S3 led to the largest deviations from the reference run in all three years.

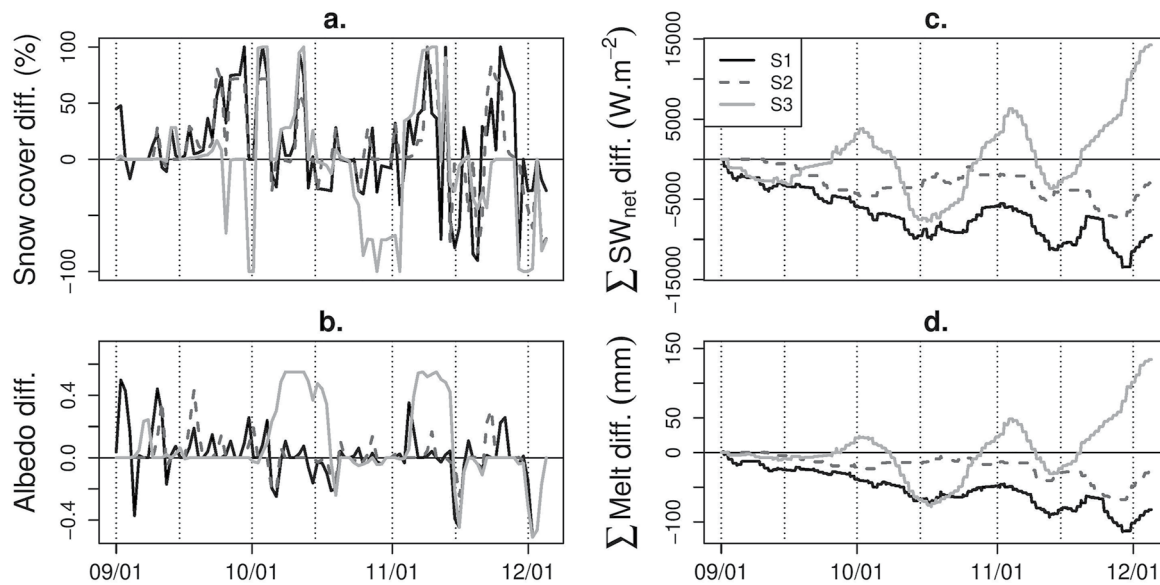


**Figure 9.** Impact of the three precipitation scenarios S1–S3 on glacier-wide (a) daily fresh snow cover area, (b) albedo, (c) net shortwave radiation and (d) melt compared to the reference run for the period September–November 2008. Results are shown as daily anomalies (a, b) and cumulative anomalies from the reference model run (c, d).

In 2004/2005, scenario S1 led to a smaller reduction in net mass loss than in the other two years because the precipitation events were already rather well distributed over time (data not shown). Compared to the reference run, the melt rate for scenario S1 was lower in September and October (Table S1 in Supporting Information S1) due to increased precipitation events. On the other hand, in November, scenario S1 resulted in six fewer precipitation events, and, combined with the fact that November is the month with the highest potential solar irradiance, there was an overall decrease in the glacier-wide albedo that significantly increased the melt rate. As a result, all the reduction in melt rate obtained between September and October was offset by the increased melt rate in the second half of November.

**Table 4**  
Summary of the Precipitation Amounts and Number of Events Above 2 mm/d Along With Simulated Surface Mass Balance (*B*) and Melt for Both the Reference Model Runs (Using Measurements Used as Model Inputs) and the Model Run Forced by the S1 Scenario) Over the Transition Period (September–November)

Years	Precipitation		Reference model run		Scenario S1 model run	
	Amounts (m)	# <i>P</i> > 2 mm/d	<i>B</i> (m w.e.)	Melt (m w.e.)	<i>B</i> (m w.e.)	Melt (m w.e.)
<i>1999/2000</i>	0.42	36	−0.12	0.55	−0.05	0.50
<i>2000/2001</i>	0.32	29	−0.39	0.67	−0.16	0.45
<b>2004/2005</b>	0.29	32	−0.99	1.23	−1.00	1.22
<i>2005/2006</i>	0.52	48	0.11	0.45	0.22	0.35
<i>2008/2009</i>	0.25	22	−0.73	0.91	−0.69	0.87
<b>2009/2010</b>	0.37	30	−0.30	0.59	−0.23	0.45
<i>2011/2012</i>	0.39	35	−0.33	0.76	−0.39	0.81
<i>2012/2013</i>	0.32	26	−0.49	0.81	−0.50	0.81
<b>2016/2017</b>	0.13	22	−0.96	1.04	−0.90	0.98
$\bar{X}$	0.33	31	−0.47	0.78	−0.41	0.72
$\sigma$	0.11	8	0.37	0.26	0.40	0.29

*Note.* The three years in italics are years in which the annual mass loss is significantly less than the average ( $B > B_{\text{mean}} + \sigma/2$ ). The three years in bold are those in which the annual mass loss is significant ( $B < B_{\text{mean}} - \sigma/2$ ).



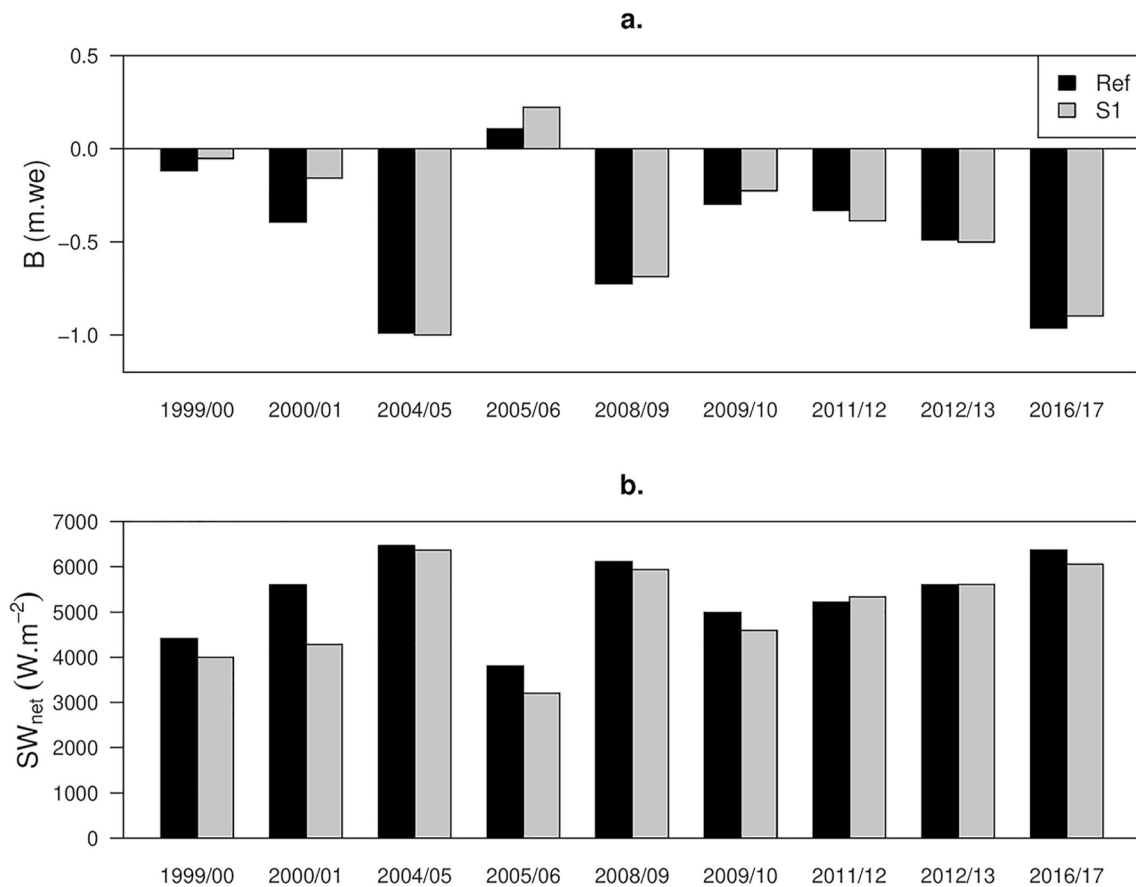


**Figure 10.** Simulated glacier-wide (a) surface mass balance and (b) net shortwave radiation over the transition period of all nine simulated years for both the reference model run and the precipitation scenario S1.

In contrast, for this year, scenario S3 reduced the net mass loss more than S1 and S2, as it allowed the formation of a thick snow-pack over the glacier. This snow-pack remained throughout the rest of the month due to numerous precipitation events of less than 2 mm/d (hence left untouched in the scenario).

Additionally, precipitation at the weather station during the transition period was lower in 2004/2005 than the nine-year average: 294 mm vs. 334 mm, partly explaining the strongly negative mass balance that year. The impact of the scenarios for the year 2004/2005 highlights the important role of the temporal distribution of precipitation in the surface mass balance variability.

Because scenario S1 was the scenario that generated the largest reduction in melt over the transition period, we applied this scenario to all nine simulated years.

#### 4.2.2. Application of Scenario S1 to All Years

Figure 10 shows the impact of S1 on the surface mass balance and net shortwave energy (plots a, b). As seen, the impact of the scenarios on the net shortwave radiation and surface mass balance are very similar: the more scenario S1 reduces the net shortwave energy balance, the smaller the surface mass loss. Averaged over the nine simulated years, scenario S1 reduced the mass loss by 0.06 m w.e. over the transition season (Figure 10a) and 0.05 m w.e. at the annual scale.

Scenario S1 reduced the net shortwave radiation on average by 9% compared to the reference runs (Figure 10b). This effect is directly linked to the fact that spreading out the precipitation events maintained a greater snow cover extent (Figure 9a) and hence a higher glacier-wide albedo (Figure 9b).

The sensible heat flux was reduced by 25% and the latent heat flux was 9% less negative compared to the reference runs. These differences are linked to the different types of glacier surface: scenario S1 yielded a larger snow

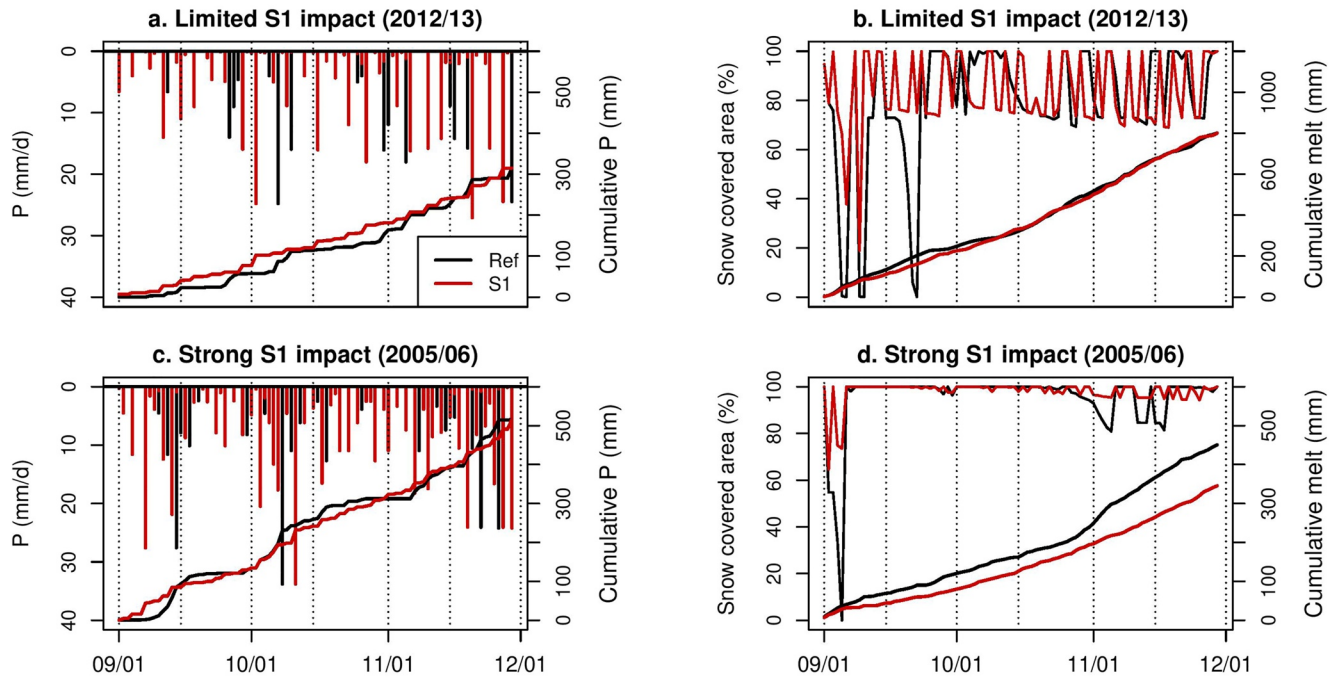


**Figure 11.** Comparison of precipitation scenario S1 model run with reference run for the transition period (September–November). (a, c) Daily and cumulative precipitation at the weather station used for model forcing. (b, d) Modeled daily glacier area with fresh snow and cumulative melt. Results are shown for a year where S1 has a limited impact (2012/2013, plots a, b) and a year where it has a strong impact (2005/2006, plots c, d).

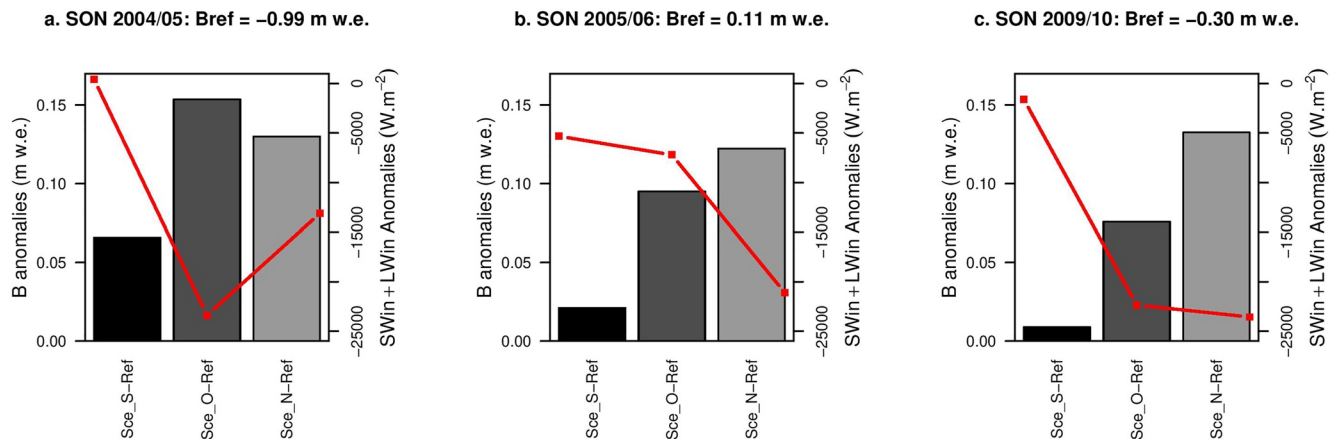
cover extent than the reference run which reduced the roughness heights of wind on the surface ( $z_{0\text{ snow}} = z_{0\text{ ice}}/10$ ). Despite these rather large differences, the turbulent fluxes remained small throughout the transition period and had a limited impact on melt rate. Finally, the impact scenario S1 had on the air temperature and relative humidity was negligible on the simulated surface mass balance.

Figure 11 illustrates the impact of scenario S1 in a year when it has a negligible impact on the surface mass balance (2012/2013, Figures 11a and 11b) and in a year when it has a significant impact (2005/2006, see Figures 11c and 11d and Table 4 for the numerical values).

In 2012/2013, because the measured precipitation events were well distributed (Figure 11a), scenario S1 results did not differ much from those of the reference run. In terms of mass loss at the monthly scale, for September and October, the scenario did not reduce the net mass loss much. In November a large precipitation event was missed (moved to October) causing the scenario to generate a higher mass loss than the reference run. Therefore, for this year, scenario S1 did not have much of an impact on the fresh snow cover and hence on the melt rate (Figure 11b). As for 2004/2005, the seasonal precipitation amount (316 mm) was below average (334 mm) partly explaining the large mass loss over the season.

Conversely, in 2005/2006, the observed precipitation events were concentrated (Figure 11c). In this case, spreading out the precipitation events maintained a thicker and larger cover of fresh snow on the glacier compared to the reference run resulting in a higher albedo and hence a lower melt rate (Figure 11d and Table 4). Significantly higher precipitation during the transition period (517 mm) than the long-term average (334 mm), contributed to a positive surface mass balance over this period.

Scenario S1 had contrasting impacts at the annual scale. For 2005/2006, scenario S1 limited mass loss more at the annual scale than over the transition period (see Table S1 in Supporting Information S1), because the snow-pack over the glacier at the end of November was thick enough to guarantee limited melt in December (until the arrival of the core wet season). On the other hand, in years when scenario S1 had a negligible impact over the transition season (e.g., 2012/2013), redistribution of the precipitation event resulted in a thinner snow-pack in December, as a result, the glacier-wide albedo decreased and the melt rate increased, resulting in greater annual mass loss. Overall, when scenario S1 increased the mass loss over the transition period, it increased the annual mass loss



**Figure 12.** Transition period surface mass balance anomalies of the cloud scenarios (scenario—reference run) for three contrasting years along with their incoming radiation fluxes.

systematically (by 5% on average). This observation highlights the combined importance of the seasonal precipitation amounts and their temporal distribution on the melt rate in the period preceding the arrival of the core wet season.

In years with large annual net mass loss (2004/2005, 2009/2010, and 2016/2017), on average, scenario S1 reduced the mass loss by 0.04 m w.e. at both transition period and annual scales. In years with limited mass loss (1999/2000, 2000/2001, and 2005/2006), net mass loss was reduced by an average of 0.14 m w.e. during the transition period and 0.15 m w.e. at the annual scale. Such marked differences between years with limited mass loss and years with significant mass loss can be explained by both precipitation amounts and by the number of events greater than or equal to 2 mm/d that occurred during the transition period. As can be seen in Table 4, years with a significant mass loss had an average of 264 mm of precipitation during the transition period in 28 events, whereas years with limited mass loss had an average of 419 mm of precipitation in 38 events.

Our investigation of the energy balance components showed that the net short-wave energy budget (via an albedo feedback effect) tends to control melt. Finally, analysis of the nine years showed that the impact of any scenario is limited if the measured precipitation events are already evenly distributed over time.

### 4.3. Sensitivity to Cloud Scenarios

Cloud scenarios had a strong impact on the surface mass balance compared to the reference runs as they systematically reduced the melt rate (Figure 12 and Figure S4 in Supporting Information S1). Averaged over all nine years, the melt rate over the transition period decreased by 6%, 15%, and 20% in the September, October, and November scenarios respectively. At the annual scale, it decreased by 2%, 5%, and 6%, respectively, thereby underlining the strong impact of clouds on surface mass balance.

As mentioned above, the November scenario limited the mass loss most. This was true for seven out of the nine years. The two exceptions were the years 1999/2000 and 2004/2005, when the October scenario limited the melt rate most. This is because these were the only two years during which there were more clear sky days in October than in November.

Although the cloud scenarios reduced the melt rate, which implied that the albedo in the ablation zone did not decay as fast as in the reference run, they had a limited impact on the glacier-wide albedo as the ablation zone represents less than 30% of the glacier surface area.

The highest observed mean difference (considering the nine-year average) in the simulated turbulent fluxes between the scenarios and the reference runs was  $-5\%$  in the October scenario. This confirms that the loss of coherence between measured parameters in the cloud scenarios has a small impact on the calculation of the turbulent fluxes.

Figure 12 shows that net mass loss during the transition period decreases as incoming radiation decreases.

Scen\_S has the least impact on the surface mass balance although September is the month with the highest average number of clear-sky days: F was largest and Tn lowest (Table 2). The limited impact can be explained by the seasonal changes in incoming radiation at the top of the atmosphere. In September, the daily mean top of atmosphere shortwave radiation ( $\pm$  standard deviation of daily values) is  $402 \pm 13 \text{ W m}^{-2}$ ,  $435 \pm 6 \text{ W m}^{-2}$  in October, and  $446 \pm 1 \text{ W m}^{-2}$  in November. Therefore, Scenario Scen\_S reduced less incoming shortwave energy than the October or November scenarios.

Thus, the cloud scenarios had a significant impact on the surface mass balance but these are probably underestimated because adding overcast conditions over the whole month would most certainly add precipitation events that would further limit the mass loss. Basic statistics linking the number of cloudy days and precipitation during the transition period in the nine years showed that there is an average of one precipitation event of 4.5 mm w.e. per 1.7 cloudy days. From this information, adding 10 cloudy days in September would add six precipitation events whereas adding six cloudy days in October and November would add three to four precipitation events.

## 5. Summary and Conclusions

A nine-year data set at hourly time scale was used as input data for a distributed energy mass balance model on Zongo Glacier. This allowed the evaluation of different processes that impact the melt rate and the mass balance.

In contrast to previous classifications based on surface mass balance variations (e.g., Rabatel et al., 2012, 2013) or precipitation and melt rates (Sicart et al., 2011), we found that three seasons (wet, dry, and transition) can be identified based on the cloud radiative properties. During the transition period, clouds have a moderate impact on the sum of the incoming short and longwave radiation fluxes with a peak distribution centered around  $-120 \text{ W m}^{-2}$ . During the wet season, the clouds have a strong attenuation impact on the incoming radiation fluxes with a peak around  $-150 \text{ W m}^{-2}$ . Such a strong impact is typical of thick (sunlight attenuating) cumulus-type clouds resulting from convective events. Finally, during the dry season, the cloud impact on the incoming radiation fluxes is low (peak around  $-20 \text{ W m}^{-2}$ ), which is typical of thin high-altitude clouds. The changes in cloud radiative properties have an impact on the melt rate especially toward the end of the transition season and during the wet season when solar attenuation is at its maximum as these offset the effect of the increased top of atmosphere radiation (as it is the austral summer).

During model calibration, we found that adjusting the DEMs and glacier contours for each year enhanced the simulation precision specifically for years with significant mass loss because, for these years, melt would otherwise be overestimated.

Melt energy and its interannual variations were maximum during October and November which means that it is a key period in controlling the annual variability of the surface mass balance. Although some energy was available during the dry season, most was converted into ground heat flux due to the intense night cooling of the glacier surface thereby shortening the daily melting period, resulting in low melt rates.

The sensitivity analysis of the distribution of the precipitation events over the transition period validated the hypothesis that the frequency of precipitation events is a key driver of the interannual variability of the surface mass balance: evenly distributed precipitation events with no change in the seasonal snow amounts maintained a larger cover of fresh snow on the glacier surface, which increased the glacier-wide albedo. As a result, the net shortwave radiation budget was reduced, in turn reducing the melt rate. The contrasting impacts on the melt rate reduction (very strong impact in years with average or above average seasonal precipitation amounts and smaller impact in years with below average precipitation) highlights the combined importance of the distribution of precipitation events over time and of the seasonal precipitation amounts.

The sensitivity analysis of the cloud cover showed that prolonged cloudy periods in October—and more particularly in November—had the potential to dramatically reduce the melt rate at both the seasonal and annual scales. A sustained cloud cover in November had more impact than in the other months of the transition period as November is the month when potential solar irradiance is close to its annual maximum.

These results emphasize the role of the onset of the wet season on the annual glacier surface mass balance as hypothesized by Sicart et al. (2011) based on the analysis of the seasonal changes of the energy fluxes during one hydrological year.

All in all, the temporal distribution of precipitation is a key driver of the interannual variability of the surface mass balance via an albedo feedback effect that reduces the net shortwave radiation budget (main driver of melt) and hence the melt rate.

The methodology used to generate the precipitation scenarios could be used to assess past and future climate over Zongo Glacier using paleoclimate proxy information or global climate model (GCM) outputs to constrain climate scenarios. Such studies would be of interest as the future of Zongo Glacier and the neighboring glaciers in the Cordillera Real of Bolivia is crucial both in terms of water supply and for hydroelectricity production.

## Data Availability Statement

The data used in this study can be found at the following link: <https://glacioclim.osug.fr/335-Energy-balance-on-a-tropical-glacier-in-Bolivia> (Autin et al., 2022).

## Acknowledgments

This study has been realized within the framework of the Andean part of the French *Service National d'Observation GLACIOCLIM* ([www.glacioclim.osug.fr](http://www.glacioclim.osug.fr), UGA-OSUG, CNRS-INSU, IRD, IPEV, INRAE), and the International Joint Laboratory LMI GREAT-ICE (IRD, EPN-Quito). The glaciological program is coordinated in La Paz by Dr. Soruco (IGEMA-UMSA) who organizes, in particular, the follow-up of the glaciological measurements in Bolivia. The authors are grateful to everyone that has been involved in the long-term in situ monitoring program on Zongo Glacier. All authors acknowledge the support of LabEx OSUG@2020 (*Investissements d'Avenir*—ANR10\_LABX56).

## References

- Abermann, J., Kinnard, C., & MacDONELL, S. (2014). Albedo variations and the impact of clouds on glaciers in the Chilean semi-arid Andes. *Journal of Glaciology*, 60(219), 183–191. <https://doi.org/10.3189/2014jog13j094>
- Autin, P., Sicart, J. E., Rabatel, A., Soruco, A., & Hock, R. (2022). Climate controls on the interseasonal and interannual variability of the surface mass and energy balances of a tropical glacier (Zongo Glacier, Bolivia, 16°S): New insights from the multi-year application of a distributed energy balance model dataset [Data Set]. Retrieved from <https://glacioclim.osug.fr/335-Energy-balance-on-a-tropical-glacier-in-Bolivia>
- Beljaars, A. C. M., & Holtslag, A. A. M. (1991). Flux parameterization over land surfaces for atmospheric models. *Journal of Applied Meteorology and Climatology*, 30(3), 327–341. [https://doi.org/10.1175/1520-0450\(1991\)030<0327:fpolsf>2.0.co;2](https://doi.org/10.1175/1520-0450(1991)030<0327:fpolsf>2.0.co;2)
- Bradley, R. S., Keimig, F. T., Diaz, H. F., & Hardy, D. R. (2009). Recent changes in freezing level heights in the tropics with implications for the deglaciation of high mountain regions. *Geophysical Research Letters*, 36(17), L17701. <https://doi.org/10.1029/2009gl0137712>
- Braun, M., & Hock, R. (2004). Spatially distributed surface energy balance and ablation modeling on the ice cap of King George Island (Antarctica). *Global and Planetary Change*, 42(1–4), 45–58. <https://doi.org/10.1016/j.gloplacha.2003.11.010>
- Cuffey, K. M., & Paterson, W. S. B. (2010). *The physics of glaciers* (Vol. 504). Amsterdam: Academic Press. Cambridge University Press (CUP).
- Cusicanqui, D., Soruco, Á., Rabatel, A., & Anthelme, F. (2015). Mass balance of Zongo Glacier between 2006 and 2013 using volumetric method, employing Pléiades high-resolution images acquired over the Cordillera Real, Bolivia (16°S, 68°W). *Revista Boliviana de Geociencias*, 8(7), 5–20.
- Dussailant, I., Berthier, E., Brun, F., Masiokas, M., Hugonnet, R., Favier, V., et al. (2019). Two decades of glacier mass loss along the Andes. *Nature Geoscience*, 12(10), 802–808.
- Espinoza, J. C., Ronchail, J., Lengaigne, M., Quispe, N., Silva, Y., Bettolli, M. L., et al. (2013). Revisiting wintertime cold air intrusions at the east of the Andes: Propagating features from subtropical Argentina to Peruvian Amazon and relationship with large-scale circulation patterns. *Climate Dynamics*, 41(7–8), 1983–2002. <https://doi.org/10.1007/s00382-012-1639-y>
- Franco, B., Ribstein, P., Saravia, R., & Tiriau, E. (1995). Monthly balance and water discharge of an inter-tropical glacier: Zongo Glacier, Cordillera Real, Bolivia, 16°S. *Journal of Glaciology*, 41(137), 61–67. <https://doi.org/10.3189/s0022143000017767>
- Franco, B., Vuille, M., Favier, V., & Cáceres, B. (2004). New evidence for an ENSO impact on low-latitude glaciers: Antizana 15, Andes of Ecuador, 0°28'S. *Journal of Geophysical Research: Atmospheres*, 109(D18).
- Garreaud, R. (2000). Intraseasonal variability of moisture and rainfall over the South American Altiplano. *Monthly Weather Review*, 128(9), 3337–3346. [https://doi.org/10.1175/1520-0493\(2000\)128<3337:ivomar>2.0.co;2](https://doi.org/10.1175/1520-0493(2000)128<3337:ivomar>2.0.co;2)
- Garreaud, R., Vuille, M., & Clement, A. C. (2003). The climate of the Altiplano: Observed current conditions and mechanisms of past changes. *Paleogeography, Paleoclimatology, and Paleoecology*, 194(1–3), 5–22. [https://doi.org/10.1016/s0031-0182\(03\)00269-4](https://doi.org/10.1016/s0031-0182(03)00269-4)
- Garreaud, R., & Wallace, J. M. (1998). Summertime incursions of midlatitude air into subtropical and tropical South America. *Monthly Weather Review*, 126(10), 2713–2733. [https://doi.org/10.1175/1520-0493\(1998\)126<2713:siomai>2.0.co;2](https://doi.org/10.1175/1520-0493(1998)126<2713:siomai>2.0.co;2)
- Gurgiser, W., Marzeion, B., Nicholson, L., Ortner, M., & Kaser, G. (2013). Modeling energy and mass balance of Shallap Glacier, Peru. *The Cryosphere*, 7(6), 1787–1802. <https://doi.org/10.5194/tc-7-1787-2013>
- Gurgiser, W., Mölg, T., Nicholson, L., & Kaser, G. (2013). Mass-balance model parameter transferability on a tropical glacier. *Journal of Glaciology*, 59(217), 845–858. <https://doi.org/10.3189/2013jog12j226>
- Hardy, D. R., Vuille, M., Braun, C., Keimig, F., & Bradley, R. S. (1998). Annual and daily meteorological cycles at high altitude on a tropical mountain. *Bulletin of the American Meteorological Society*, 79(9), 1899–1913. [https://doi.org/10.1175/1520-0477\(1998\)079<1899:aadmca>2.0.co;2](https://doi.org/10.1175/1520-0477(1998)079<1899:aadmca>2.0.co;2)
- Hastenrath, S. (1997). Measurements of diurnal heat exchange on the Quelccaya Ice Cap, Peruvian Andes. *Meteorology and Atmospheric Physics*, 62(1), 71–78. <https://doi.org/10.1007/bf01037480>
- Hock, R. (1998). *Modeling of glacier melt and discharge*. (Doctoral dissertation). Retrieved from <http://www.agu.org/pubs/cross-ref/2009/2009JD011949.shtml>
- Hock, R., & Holmgren, B. (2005). A distributed surface energy-balance model for complex topography and its applications to Storglaciären. *Journal of Glaciology*, 51(172), 25–36.
- Hock, R., & Tijm-Reijmer, C. (2012). *A mass-balance, glacier runoff, and multi-layer snow model DEBAM and DETIM distributed energy balance and distributed enhanced temperature index model users manual [software manual]*. Retrieved from <http://www2.gi.alaska.edu/~regine/modelmanual.pdf>
- Hurley, J. V., Vuille, M., & Hardy, D. R. (2016). Forward modeling of  $\delta^{18}\text{O}$  in Andean ice cores. *Geophysical Research Letters*, 43(15), 8178–8188. <https://doi.org/10.1002/2016gl070150>
- Kaser, G. (1999). A review of the modern fluctuations of tropical glaciers. *Global and Planetary Change*, 22(1–4), 93–103. [https://doi.org/10.1016/s0921-8181\(99\)00028-4](https://doi.org/10.1016/s0921-8181(99)00028-4)

- Kaser, G. (2001). Glacier-climate interaction at low latitudes. *Journal of Glaciology*, 47(157), 195–204. <https://doi.org/10.3189/172756501781832296>
- Kaser, G., Ames, A., & Zamora, M. (1990). Glacier fluctuations and climate in the Cordillera Blanca, Peru. *Annals of Glaciology*, 14, 136–140. <https://doi.org/10.1017/s0260305500008430>
- Lejeune, Y., Wagnon, P., Bouilloud, L., Chevallerier, P., Etchevers, P., Martin, E., et al. (2007). Melting of snow cover in a tropical mountain environment in Bolivia: Processes and modeling. *Journal of Hydrometeorology*, 8(4), 922–937. <https://doi.org/10.1175/jhm590.1>
- Lenters, J. D., & Cook, K. H. (1997). On the origin of the Bolivian high and related circulation features of the South American climate. *Journal of the Atmospheric Sciences*, 54(5), 656–678. [https://doi.org/10.1175/1520-0469\(1997\)054<0656:otootb>2.0.co;2](https://doi.org/10.1175/1520-0469(1997)054<0656:otootb>2.0.co;2)
- Litt, M., Sicart, J. E., Helgason, W. D., & Wagnon, P. (2014). Turbulence characteristics in the atmospheric surface layer for different wind regimes over the tropical Zongo Glacier (Bolivia, 16°S). *Boundary-Layer Meteorology*, 154(3), 471–495. <https://doi.org/10.1007/s10546-014-9975-6>
- Masiokas, M. H., Rabatel, A., Rivera, A., Ruiz, L., Pitte, P., Ceballos, J. L., et al. (2020). A review of the current state and recent changes of the Andean cryosphere. *Frontiers in Earth Science*, 8(99), 1–27. <https://doi.org/10.3389/feart.2020.00099>
- Maussion, F., Gurgiser, W., Großhauser, M., Kaser, G., & Marzeion, B. (2015). ENSO influence on unstable energy and mass balance at Shallap Glacier, Cordillera Blanca, Peru. *The Cryosphere*, 9(4), 1663–1683. <https://doi.org/10.5194/tc-9-1663-2015>
- Mölg, T., Cullen, N. J., Hardy, D. R., Kaser, G., & Klok, L. (2008). Mass balance of a slope glacier on Kilimanjaro and its sensitivity to climate Thomas. *International Journal of Climatology*, 28(6), 881–892. <https://doi.org/10.1002/joc.1589>
- Mölg, T., Cullen, N. J., & Kaser, G. (2009). Solar radiation, cloudiness and longwave radiation over low-latitude glaciers: Implications for mass-balance modeling. *Journal of Glaciology*, 55(190), 292–302. <https://doi.org/10.3189/002214309788608822>
- Nicholson, L. I., Prinz, R., Mölg, T., & Kaser, G. G. (2013). Micrometeorological conditions and surface mass and energy fluxes on Lewis Glacier, Mt Kenya, in relation to other tropical glaciers. *The Cryosphere*, 7(4), 1205–1225. <https://doi.org/10.5194/tc-7-1205-2013>
- Oerlemans, J., & Knap, W. H. (1998). A one year record of global radiation and albedo in the ablation zone of Morteratschgletscher, Switzerland. *Journal of Glaciology*, 44(147), 231–238. <https://doi.org/10.1017/s0022143000002574>
- Østby, T. I., Schuler, T. V., Hagen, J. O., Hock, R., Kohler, J., & Reijmer, C. H. (2017). Diagnosing the decline in climatic mass balance of glaciers in Svalbard over 1957–2014. *The Cryosphere*, 11(1), 191–215. <https://doi.org/10.5194/tc-11-191-2017>
- Paulson, C. A. (1970). The mathematical representation of wind speed and temperature profiles in the unstable atmospheric surface layer. *Journal of Applied Meteorology and Climatology*, 9(6), 857–861. [https://doi.org/10.1175/1520-0450\(1970\)009<0857:tmrows>2.0.co;2](https://doi.org/10.1175/1520-0450(1970)009<0857:tmrows>2.0.co;2)
- Prinz, R., Nicholson, L. I., Mölg, T., Gurgiser, W., & Kaser, G. (2016). Climatic controls and climate proxy potential of Lewis Glacier, Mt. Kenya. *The Cryosphere*, 10(1), 133–148. <https://doi.org/10.5194/tc-10-133-2016>
- Rabatel, A., Bermejo, A., Loarte, E., Soruco, A., Gomez, J., Leonardini, G., et al. (2012). Can the snowline be used as an indicator of the equilibrium line and mass balance for glaciers in the outer tropics? *Journal of Glaciology*, 58(212), 1027–1036.
- Rabatel, A., Francou, B., Soruco, A., Gomez, J., Cáceres, B., Ceballos, J. L., et al. (2013). Current state of glaciers in the tropical Andes: A multi-century perspective on glacier evolution and climate change. *The Cryosphere*, 7(1), 81–102. <https://doi.org/10.5194/tc-7-81-2013>
- Ramallo, C. (2013). *Caractérisation du régime pluviométrique et sa relation à la fonte du Glacier Zongo (Cordillère Royale)*, (Doctoral dissertation). Retrieved from <https://tel.archives-ouvertes.fr/tel-01548283>
- Reijmer, C. H., & Hock, R. (2008). Internal accumulation on Storglaciären, Sweden, in a multi-layer snow model coupled to a distributed energy- and mass-balance model. *Journal of Glaciology*, 54(184), 61–72. <https://doi.org/10.3189/002214308784409161>
- Ribstein, P., Tiriau, E., Francou, B., & Saravia, R. (1995). Tropical climate and glacier hydrology: A case study in Bolivia. *Journal of Hydrology*, 165(1–4), 221–234.
- Ronchail, J. (1989). Climatological winter effects of southern advections in Bolivia and north-west Brazil (1973–1984). In *The Third International Conference on Southern Hemisphere Meteorology and Oceanography*. Argentina.
- Seehaus, T., Malz, P., Sommer, C., Soruco, A., Rabatel, A., & Braun, M. (2020). Mass balance and area changes of glaciers in the Cordillera Real and Tres Cruces, Bolivia, between 2000 and 2016. *Journal of Glaciology*, 66(255), 124–136.
- Sicart, J. E. (2002). *Contribution à l'étude Des Flux d'énergie, Du Bilan de Masse et Du Débit de Fonte d'un Glacier Tropical: Le Zongo, Bolivie*, (Doctoral dissertation). Retrieved from <http://hydrologie.org/THE/SICART.pdf>
- Sicart, J. E., Espinoza, J. C., Quéno, L., & Medina, M. (2016). Radiative properties of clouds over a tropical Bolivian Glacier: Seasonal variations and relationship with regional atmospheric circulation. *International Journal of Climatology*, 36(8), 3116–3128. <https://doi.org/10.1002/joc.4540>
- Sicart, J. E., Hock, R., Ribstein, P., & Chazarin, J. P. (2010). Sky longwave radiation on tropical Andean Glaciers: Parameterization and sensitivity to atmospheric variables. *Journal of Glaciology*, 56(199), 854–860.
- Sicart, J. E., Hock, R., Ribstein, P., Litt, M., & Ramirez, E. (2011). Analysis of seasonal variations in mass balance and Melt water discharge of the tropical Zongo Glacier by application of a distributed energy balance model. *Journal of Geophysical Research*, 119(D13), 1–18. <https://doi.org/10.1029/2010jd015105>
- Sicart, J. E., Ribstein, P., Chazarin, J. P., & Berthier, E. (2002). Solid precipitation on a tropical glacier in Bolivia measured with an ultrasonic depth gauge. *Water Resources Research*, 38(10), 7-1–7-7. <https://doi.org/10.1029/2002wr001402>
- Sicart, J. E., Wagnon, P., & Ribstein, P. (2005). Atmospheric controls of the heat balance of Zongo Glacier (16°S, Bolivia). *Journal of Geophysical Research: Atmospheres*, 110(12), 1–17. <https://doi.org/10.1029/2004jd005732>
- Soruco, A., Vincent, C., Francou, B., Ribstein, P., Berger, T., Sicart, J. E., et al. (2009). Mass balance of Glacier Zongo, Bolivia, between 1956 and 2006, using glaciological, hydrological and geodetic methods. *Annals of Glaciology*, 50(50), 1–8. <https://doi.org/10.3189/172756409787769799>
- Soruco, A., Vincent, C., Rabatel, A., Francou, B., Thibert, E., Sicart, J. E., & Condom, T. (2015). Contribution of glacier runoff to water resources of La Paz City, Bolivia (16°S). *Annals of Glaciology*, 56(70), 147–154. <https://doi.org/10.3189/2015aog70a001>
- Troll, C. (1941). *Studien zur vergleichenden Geographie der Hochgebirge der Erde* (Vol. 21). Bonn, Germany: Bonner Mitt.
- Vincent, C., Soruco, A., Azam, M. F., Basantes-Serrano, R., Jackson, M., Kjøllmoen, B., et al. (2018). A nonlinear statistical model for extracting a climatic signal from glacier mass balance measurements. *Journal of Geophysical Research: Earth Surface*, 123(9), 2228–2242. <https://doi.org/10.1029/2018jfe004702>
- Vuille, M., Francou, B., Wagnon, P., Juen, I., Kaser, G., Mark, B., & Bradley, R. S. (2008). Climate change and tropical Andean Glaciers: Past, present, and future. *Earth-Science Reviews*, 89(3–4), 79–96.
- Wagnon, P., Ribstein, P., Francou, B., & Pouyaud, B. (1999). Annual cycle of energy balance of Zongo Glacier, Cordillera Real, Bolivia. *Journal of Geophysical Research*, 104(D4), 3907–3923. <https://doi.org/10.1029/1998jd200011>
- Zemp, M., Huss, M., Thibert, E., Eckert, N., McNabb, R., Huber, J., & Cogley, J. G. (2019). Global glacier mass changes and their contributions to sea-level rise from 1961 to 2016. *Nature*, 568(7752), 382–386. <https://doi.org/10.1038/s41586-019-1071-0>